STUDIES OF SEA ICE THICKNESS AND CHARACTERISTICS FROM AN ARCTIC SUBMARINE CRUISE
Phase 3

A Progress report on work accomplished under
Contract N00014-89-C-0014 between
October 1 1988 and June 30 1989

SAIC Polar Oceans Associates
Block A2, Westbrook Centre
Milton Road
Cambridge CB4 1YQ

September 4, 1989

DISCLAIMER NOTICE

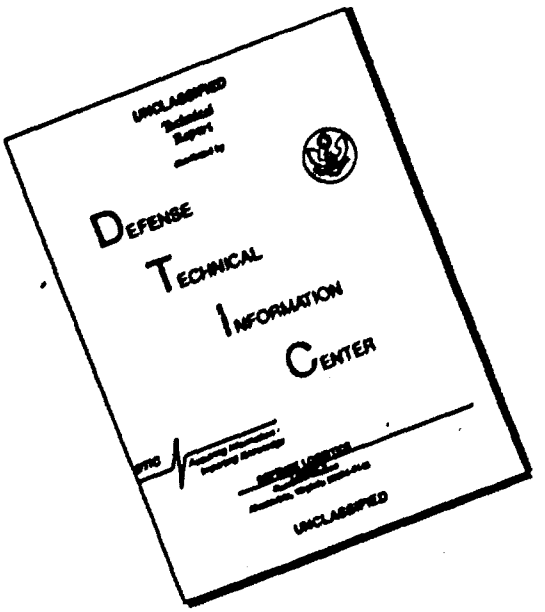

THIS DOCUMENT IS BEST QUALITY AVAILABLE. THE COPY FURNISHED TO DTIC CONTAINED A SIGNIFICANT NUMBER OF PAGES WHICH DO NOT REPRODUCE LEGIBLY.

1. INTRODUCTION

In May 1987 a unique collaborative experiment took place in the Arctic Ocean, when a British submarine and two remote sensing aircraft co-operated in concurrent profiling and imaging of the upper and lower sea ice surfaces along the same track. Dr. Peter Wadhams carried out the scientific programme from the submarine, which was equipped with a 780 upward-looking sonar system (narrow beam, 48 kHz) feeding chart and digital recorders, and an EDO Western 602 sidescan sonar towfish (100 kHz) feeding an EDO 706 sidescan mapping system. The two remote sensing aircraft comprised:

a) A NASA P-3A equipped with
   i Advanced Multichannel Microwave Radiometer (AMMR) with 37GHz and 18GHz dual polarised channels and 21GHz vertically polarised channel;
   ii Electrically Scanning Microwave Radiometer (ESMR) operating at 19GHz;
   iii Airborne Oceanographic Lidar (AOL);
   iv PRT-5 infra-red radiometer;
   v aerial cameras and video;
b) A Cessna Conquest of Intera Technologies Ltd.,Calgary, equipped with the Intera STAR-2 X-band HH-polarised synthetic aperture radar (SAR), giving a 63km swath width.

Dr J C Comiso (NASA Goddard) was in charge of the P-3A mission and Dr R T Lowry (Intera) of the SAR mission, which was funded by the Admiralty Research Establishment.

The experiment provided unique opportunities for validation of remote sensing systems using ice of known type and thickness, and for individual and comparative statistical analyses of ice thickness and roughness. This report describes analyses carried out during Phase 3 of the ONR-funded project to interpret data from this experiment. For completeness the reporting period is taken back to 1 October 1988, although a short report for the period up to 31 December 1988 was sent by telemail to ONR on 19 January 1989.

2. REGISTRATION AND DATA DISSEMINATION

From the outset it was decided that the datasets would be worked on by an analysis team drawn from SAIC Polar Oceans Associates (submarine and SAR data), NASA Goddard and Wallops (P-3A data), and NASA JPL (aerial photography and SAR registration). The team would hold regular meetings to review progress, at which representatives of the funding agencies involved (NASA, ONR, ARE) would also be present.

The first major task was co-registration of datasets. The submarine had spent 10 days operating independently in the Arctic, collecting upward-looking sonar data and terminating at the North Pole. There were then 23 days of concurrent submarine and aircraft profiling, running southward from the Pole towards Greenland, then eastward towards Fram Strait, with a final collaborative day in running southward through the East Greenland pack ice. During these periods the submarine and two aircraft navigated by inertial navigation systems (INS), with additional information from the Global Positioning System (GPS) for the P-3A during part of each day. It was decided that two types of co-registration were necessary:

i General co-registration of the entire datasets, i.e. laying out the profiles and images on a latitude/longitude basis;

ii Detailed co-registration of selected portions of track, i.e. as exact a determination as possible of the mutual tracks of the three platforms, with the purpose of performing detailed correlations of datasets, on a point-by-point basis if possible. It was decided that the first portion to be selected was a stretch of about 200km of track from north of Greenland at about 85°N, profiled on May 20th.

The general co-registration for the submarine, involved conversation of the 780 upward-looking sonar record from a function of time to a function of distance. This was accomplished using recorded position fixes for the submarine, together with measured curves of acceleration and deceleration during times of speed change.

The detailed registration procedure involved using GPS and high-altitude photography information to register the P-3A sensor data to the SAR imagery by matching recognisable leads. This was carried out by NASA, and is described more

fully in Wadhams et al. (1989). SAIC Polar Oceans Associates then co-registered the submarine track with the SAR imagery by the use of the sidescan sonar record to match features with the SAR. Leads, edges of floes, distinctive pressure ridge patterns and areas of first- and multiyear ice were all recognisable in a similar fashion both on the sidescan (for example Wadhams, 1988 and on the SAR), enabling the submarine track to be superimposed on the SAR image. SAIC used GEMS image processing system for this task. Thus, the SAR image (which is a swath-based on the Cessna flight track) became the matrix on which both the P-3A and submarine tracks were superimposed. Any sinuosity in the track of the Cessna was therefore folded into the tracks of the submarine and NASA aircraft.

Detailed registration of the 200km sample of track permitted systematic comparisons of sensor outputs to be carried out. The team carrying out this work held two meetings during the period covered by this report, to review process and plan further analyses. The first meeting was held in Cambridge from 8-10 November 1988, and the proceedings are given as Appendix 1 of this report. In addition to scientific work, an understanding was reached at this meeting regarding a policy on data release.

In December 1988 Wadhams, Comiso and Crawford met at the AGU Fall Meeting in San Francisco to review progress. The second major workshop was held at NASA Wallops on 27-28 March 1989, with six attendees (Wadhams, Comiso, Krabill, Swift, Tucker and Crawford). Proceedings are given as Appendix 2. A paper was completed, and tasks for a second paper agreed. The first paper (Wadhams et al. 1989) is enclosed here in Appendix 4. The second paper, Comiso et al. (1989) has now been prepared for submission for publication. This paper is due for submission at the end of August In addition, Wadhams and Martin gave a paper at the December 1988 AGU. This is to be published by CRREL and is enclosed in Appendix 4.

3. ANALYSIS OF SUBMARINE DATA

3.1 780 Upward-looking Sonar

3.1.1 Data quality

Upward-looking sonar profiles were obtained using the 780 system with a transducer on the top of the submarine fin. The 780 system has a beam width of approximately 10°. The effective footprint of the beam on the ice bottom was about 15m. Thus, the first return from an emitted pulse comes from the point on the ice underside, lying within a cone of angle 10° and at minimum range from the transducer. This does not necessarily correspond with the point lying directly above the transducer. Nevertheless, at least in undeformed ice, the strongest echo can be expected to come from the central part of the beam.

The chart record often contained fainter echoes at lower range than the normal strong continuous echo and it can be assumed that these came from steeply inclined ice surfaces in the outer part of the beam footprint. It appeared that the digitiser tended not to respond to such faint returns and gave an output which was fixed on the strongest echo. Thus, to some extent, the use of the digitised record compensated for problems associated with beamwidth effects. It is assumed that the digitised record, as used for statistical analysis, is a correct profile of the range to the ice bottom directly above the submarine. Further discussion of beamwidth problems and their solution is given in Wadhams (1981).

3.1.2 Data reduction

The first stage, in data reduction used the chart record to insert data wherever the digitiser lost lock and failed to record the ice surface. This occasionally happened for short periods, usually due to a steep ice ridge. The procedure was to plot out the digital record with the same scaling (depth, time) as the chart record, manually digitise short sections of chart record wherever required and merge these into the digital dataset.

The second step, was to convert range into draught by removing the profile of submarine depth variations. This was done by identifying points on the record (using the

charts) that were definitely open water, identifiable by very strong echoes (often containing multiple returns). These points were joined by a smooth polynomial, which was then subtracted from the range to leave a record of draught versus time.

The third step, required the convesion of the draught versus time into a record of draught versus distance, which was achieved using the speed log of the submarine. A Ships Inertial Navigation System (SINS) log of position versus time (recorded at approximately 10 minute intervals by the sidescan sonar watchkeeper) was used. This was combined with manually observed acceleration-deceleration data to give a continuous speed-time curve, which was then applied to the data points, which had been digitally recorded at a rate of 4.6875 points per second (the ping rate of the sonar). Finally, the record was quadratically interpolated to yield a record of ice draughts at 1m horizontal intervals.

The 1m ice draught record was then statistically analysed in 50km along track sections. These usually contained slightly less than 50km of data, because of times when the sonar was turned off for cleaning or roll changes. The total record length was 3,400km. The section numbers run from 1 to 68.

3.1.3 Statistical analysis

We now refer to the line printer output example (for 50km Section 1) shown in Appendix 3 and supply a commentary to each of the statistics that are presented.

Ice draught distribution - 50km section

The probability density function of ice draught. A bin size of 10cm is used, and the probabilities are normalised so that the total is 100,000. It will be noted that some points lie in negative bins (from -1m to 0m). These are almost all open water points where there has either been a slight mismatch between the depth-keeping polynomial and the real depth, or else the random error produced by the detection circuits within the digitiser has pushed some points over into apparent negative depths Very little additional error is introduced if these points are set to zero depth, but we retain the negative values here in order to avoid bias error in computing mean values.

The ice draught distributions are then summed in 50cm and 1m depth bins, in order to give a coarser but clearer indication of the frequency distribution.

Sea ice draught statistical parameters

i modal draught, this is the draught bin with the highest probability
ii mean draught
iii root mean square (rms) draught
iv variance about mean
v standard deviation
vi median draught is the value of the middle point when all the draught points are ranked.

These parameters are recalculated with negative draught values set to zero.

Polynya/lead distribution - 50km section

A polynya or lead is defined here as a continuous sequence of depth points, none of which exceed a value of 0.5m, 0.75m or 1m. These three criteria are used in order to distinguish between leads which are at different stages of re-freezing.

The leads are classified not only by ice draught but also by along track lead width in 10m intervals up to 100m, then in 20m intervals up to 200m and 50m intervals up to 1000m.

Two tabulations are given. One shows the number of leads per 100km. The other is of actual lead numbers encountered in the section.

Lead/polynya analysis statistical parameters

For each of the depth criteria of 0.5m, 0.75m and 1m:

i mean number of leads encountered per 100km of track
ii mean lead width along track (m)
iii rms lead width along track (m)
iv variance of lead width, (m^2)
v standard deviation of lead width (m)
vi median lead width (m).

These statistics are repeated, zeroing negative depth values. The results are identical, excepting rounding errors.

Conditional probability of leads/polynya

For each draught criterion, the fraction of the total number of leads occurring in each width range is given (normalised to 100,000).

Level/rough ice distribution - 50km section

'Smooth ice' and 'rough ice' are distinguished on the basis that 'smooth ice' consists of a continuous sequence of depth points, at least 10m in length, in which the bottom surface slope is always less than 0.05. Therefore, there is always less than 5cm depth difference between successive points. Experiments have shown that this criterion offers the best approximation to the choice made by the human eye when it examines an ice profile and attempts to distinguish between undeformed ice (bottoms of floes and refrozen leads) and deformed ice (pressure ridges and rubble fields).

Analysis of smooth ice - 50km section

The percentage of the ice profile occupied by smooth ice is given.

Smooth ice distribution - 50km section

A probability density function of smooth ice draught, in 10cm draught bins from -1 to 50m, normalised to a total of 100,000 points.

The next table shows the same distribution binned more coarsely in 0.5m and 1m depth categories.

These distributions reflect the preferred draughts reached by undeformed ice of varying ages. The relative percentages of young, firstyear and multiyear ice in the record can then be estimated. Young ice is usually less than 1m thick and firstyear ice less than 2m thick. The 10m minimum length criterion for sections of smooth ice protects against erroneous identification of pressure ridge crests and other turning points as being 'smooth ice'.

Smooth ice statistical parameters

Identical parameters as those for the whole record are shown.

Analysis of rough ice. 50km section

These are the inverse of the smooth ice statistics. 'Rough ice' is defined as all the ice that is not smooth ice. Rough ice sections can therefore be shorter than 10m.

All of the same statistics are generated as for smooth ice.

Level/rough ice length/draught analysis

This is a complete breakdown of the 50km record, showing the length of each section of level ice and its mean draught, followed by the length and mean draught of the succeeding section of rough ice. The intention here is twofold. For central Arctic data, these results enable us to simulate acoustic transmission loss by assigning different acoustic reflectivities to rough ice. Level multiyear ice (more than 2m thick and having a characteristic bottom of gentle bulges, Wadhams, 1988) and level firstyear ice (very smooth bottom). For the Marginal Ice Zone (MIZ), the level ice section lengths correspond to along track floe diameters.

Distribution of segment lengths (m)

The number of segments (per 100km of track) in 50m bins of segment length are given.

Distribution of mean draughts (m)

These are the numbers of segments (per 100km) and total segment lengths in 0.5m categories of mean draught. In the case of level ice, this is another way of identifying the preferred age of undeformed ice.

Analysis of pressure ridges - draught and spacing

An independent pressure ridge is identified by a Rayleigh criterion algorithm. The depth of the crest is compared with the depths of the troughs (minimum points) on either side of it. If the troughs each regress more than half way towards an arbitrary 'level ice horizon', (chosen to be 2.5m), the ridge is classed as independent and is counted in the statistics. If not, the crest is regarded as a local peak which forms part of the 'foothills' of a deeper keel on one side or the other. This is similar to the

Rayleigh criterion for resolving spectral lines. Some implications of this definition are discussed in Lowry and Wadhams (1979).

Listing of ridge draught and spacing - 50km section

Each ridge in the record is listed with its draught and the spacing to the crest of the next ridge.

Distribution of pressure ridge draughts (-1.0m - 50m)

The number of pressure ridges in the record and the number per 100km, are listed in 1m increments of draught.

Statistical parameters - total pressure ridges

i total number of pressure ridges in a record
ii number per km of track
iii mean draught (m)
iv rms draught (m)
v variance (m^2)
vi standard deviation (m)
vii median draught (m)

The same parameters follow for ridges which are deeper than 5m and ridges which are deeper than 9m. This eliminates 'ridges' which are really discrete ice floes, and shows the numbers of genuine pressure ridges present. In the MIZ the number of ridges deeper than 9m is quite small, because of bottom melting.

Pressure ridge - maximum draught

This is also the maximum ice draught occurring in the 50km record.

Distribution of pressure ridge spacing

The number of ridges per 100km track, the probability and the cumulative probability, are shown for 20m categories of spacing up to 400m. This is intended as a test of the result found by Wadhams and Davy (1986), that pressure ridge spacings in the central Arctic fit a lognormal distribution.

Regression correlation coefficients

Various distributions (lognormal, negative exponential, logarithmic and exponential lognormal) are applied to the ridge spacing statistics and correlation coefficients calculated. In the case of MIZ ice, it appears that the negative exponential distribution usually offers a better fit than the lognormal.

3.1.4 Interpretation

A typical set of results from a 50km section (Section 1, starting from the North Pole) is enclosed as Appendix 3. Overall, data from 68 x 50km sections have been analysed in this way, covering 3400km of ice from the North Pole to the Greenland Sea ice edge, with data processing on the records collected before the North Pole visit still in progress. Results are being interpreted in detail and confirm many earlier findings, e.g.

i negative exponential distribution for ridge draughts;
ii negative exponential or lognormal distribution for ridge spacings;
iii thicker ice off North Greenland than in central Arctic; thinnest ice in Greenland Sea;
iv lead width and spacing distributions fit no simple statistical law.

A paper on the complete statistical interpretation of these data, and their comparison with earlier datasets, is in preparation. Statistics corresponding to the intensively analysed ice section have been reported (Comiso **et al.** 1989 and Section 4 below).

3.2 Wave Number Spectra

A separate analysis was carried out for energy spectra of the under-ice surface. The wave number spectrum of the ice underside is of considerable importance since it is the basis of the method of small perturbation (MSP), a theoretical technique for estimating the sound scattering loss from the ice surface (Lysanov, 1974; Bass and Fuks, 1979; Guoliang and Wadhams, 1989. It is also the basis of some theoretical approaches to the problem of internal wave generation under ice (R. Pinkel, pers. comm.). Wave number

spectra were computed for each of the 50km sections of sonar data, and some extremely interesting results have been obtained.

Figure 1 shows the average of 38 spectra of 50km sections drawn from the Arctic interior. Each under-ice record was sampled at 12m intervals. Thus, the spectra are calculated up to the Nyquist frequency of $0.5m^{-1}$. Under-ice records from the marginal ice zone region typically show spectra where the energy density varies as k^{-3}. This is exemplified by Figure 2 here, taken from Guoliang and Wadhams (1989), which represents data collected on a submarine 1985 cruise. However, there is no sign of such a variation in the ice interior (figure 1). Instead, the energy density varies as roughly k^{-4} for short wavelengths (less than 11 m) and as k^{-2} or even k^{-1} at longer wavelengths. There is a distinct 'knee' at 11m wavelength, visible in most of the individual 50km sections. This appears to be unrelated to either the beam diameter (8m or less) or any wavelength of platform porpoising. The knee may be a genuine feature of the ice bottom roughness, marking the wavelength where the roughness due to individual ice blocks on the underside gives way to the roughness due to entire ice features such as ridges and floes. Further research is in progress on these data and will be reported in the final data report on this project and/or in an associated paper.

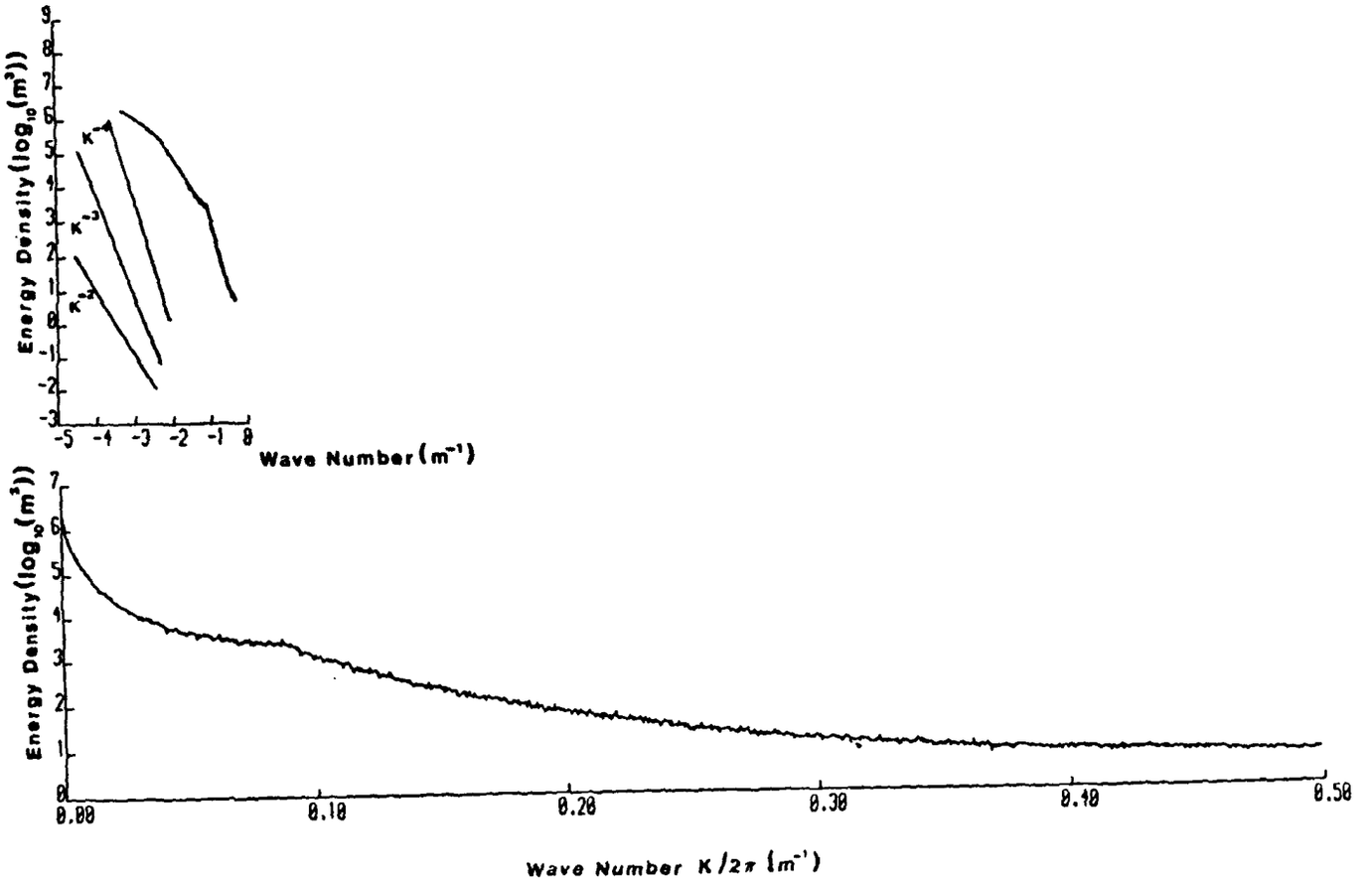

Figure 1. Mean wave number spectrum from 38 50km sections in central Arctic. K^{-2}, K^{-3}, K^{-4} decay lines are shown for comparison.

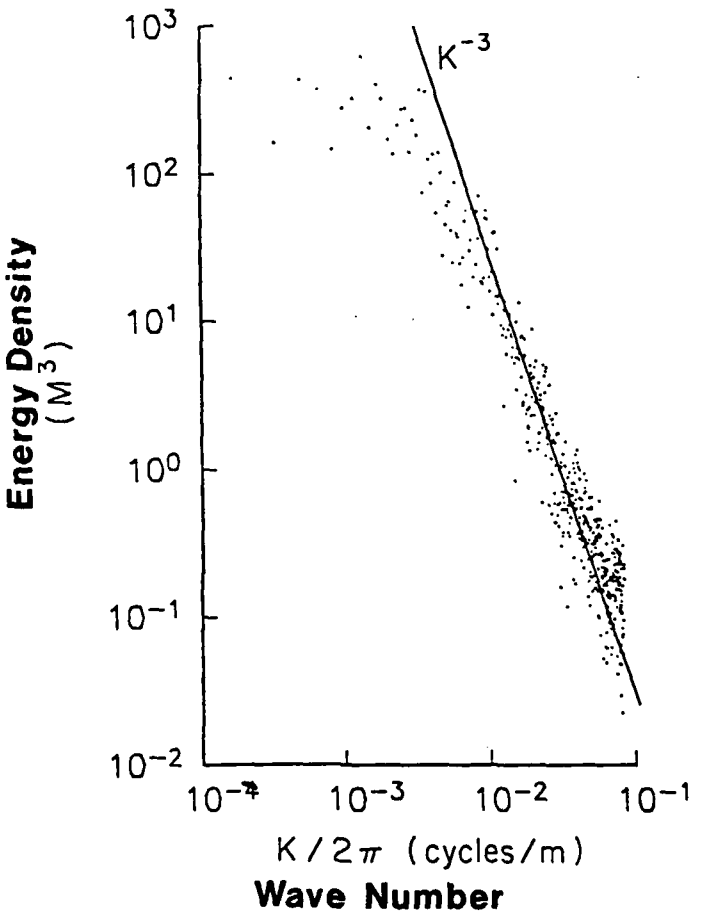

Figure 2. Wave number spectrum from the marginal ice zone in the Greenland Sea (from Guoliang and Wadhams, 1989).

3.3 Sidescan Sonar Analysis

The sidescan sonar data were recorded on electrically sensitive paper, giving a fragile analogue record. Back-up recording was on analogue magnetic tape which requires replaying through an EDO recorder. Wherever the submarine was sailing at less than 8 kts it was possible for the watchkeeper to input the submarine speed into the recording system,, which changed the rate of progress of the chart paper. Similarly, when the submarine's depthkeeping was steady it was easy to input the depth into the recorder. These two inputs generated a chart record which was geometrically correct, i.e. compensated for both depth (range transformed into lateral distance) and speed.

When depthkeeping was poor (e.g. during exercises) the surface correction was imperfect, producing a blank area or a loss of data at the centre of the image (further minor mismatches were caused by the boat's list). More importantly, when the submarine was travelling at more than 8 kts it was not possible to produce a genuinely correct record as the chart speed could not be further increased. Also, there were gaps between the coverage of the ice between successive pulses, so the record was not only distorted but degraded. When these conditions occurred a chart speed setting was used which was a simple sub-multiple (1:2, or 1:4) of the submarine speed.

Of 3000km of sidescan record obtained, some 1000km were of 'good' quality (i.e. geometrically correct) and 2000km of 'poor' quality. In the analysis, emphasis was given to the good quality data. First, the entire dataset was photographed to ensure its preservation. Three sorts of analysis were then carried out:

(a) Comparative analyses with aircraft datasets (with SAR for registration purposes; with AMMR; with ESMR). These are described elsewhere in this report.

(b) Comparative analyses with upward sonar data:
  (i) Individual ridges were identified in sidescan and 780 upward-looking sonar records. The angle at which a ridge crossed the submarine track was measured on the sidescan, and the apparent slope angles of the ridge measured on 780 upward-looking sonar. The crossing angle was used to correct the

apparent slopes so as to yield a true distribution of ridge slopes. This was used to test the hypothesis that ridges are isotropic, and that a random orientation assumption can be used to convert an apparent into a true ridge slope distribution in the manner described by Wadhams (1978).

(ii) A similar analysis was carried out of lead orientations and widths, to convert an apparent lead width distribution into a true lead width distribution.

Work is still in progress on (b) and will be reported in the final report.

(c) Internal analysis of sidescan sonar data. An important discovery to emerge from Phase 3 was that the underside of undeformed multiyear ice has a quite different appearance from that of undeformed firstyear ice (Wadhams, 1988). Multiyear ice has a bottom composed of blisters or bulges with typical relief of 1m and diameter 10 to 80m, while firstyear ice has a smooth bottom criss-crossed by narrow cracks. This difference was used to characterise the ice bottom into areas of undeformed multiyear; undeformed firstyear; ridged ice; and leads. Such a map not only gives percentages of each ice type but also can be used as a matrix for simulations of acoustic transmission loss, since a reflection coefficient can be ascribed to each ice type. This work is also still in progress.

4. SONAR/LASER COMPARISONS

As part of the intensive analysis reported in Comiso et al. (1989), a joint statistical analysis was carried out of three consecutive, corresponding 20km sections of ULS and laser data. Sonar statistics were calculated as described in Section 3.1, and laser statistics were calculated in a similar fashion. A result of critical importance was obtained.

The result arose from analysis of the probability density functions (pdfs) of ice draught and elevation. The sections will be designated 1, 2 and 3. The individual pdfs were plotted (Figure 3) and show little variation between the three sections and no apparent association between the two sets of distributions. Since the three sections were consecutive and retrieved from almost identical ice conditions (the heavily ridged zone north of Greenland) this is to be expected. We combined Sections 1, 2 and 3 into a single 60km section and examined the pdfs.

The first test was to compare the overall mean draught of Sections 1, 2 and 3 with the overall mean elevation. The result was a ratio of 7.909. This ratio R should be related to mean ice and surface water densities ρ_i and ρ_w by

$$R = \frac{\rho_i}{\rho_w + \rho_i} \qquad (1)$$

If we assume a surface water density of 1025kg m^{-3} (typical of Arctic surface water before melt beings) then this gives a mean ice density of 910kg m^{-3},close to the value found by Wadhams (1981) of 915kg m^{-3} by a similar draught/elevation comparison on ULS and laser data.

The draught and elevation distributions were plotted together, but with the horizontal scale of the elevation distribution expanded by a factor of 7.909, and the vertical scale compressed to yield the same area under the curve. The result (Figure 4) of this co-ordinate transformation is such a close agreement that we can conclude that the ice cover behaves as if surface features were magnified by a factor R on the underside. in other words, if a fraction F(h) of the ice cover has an elevation in the range h to (h+dh), then the same fraction F(h) will have a draught in the range 7.909h to 7.909(h+dh).

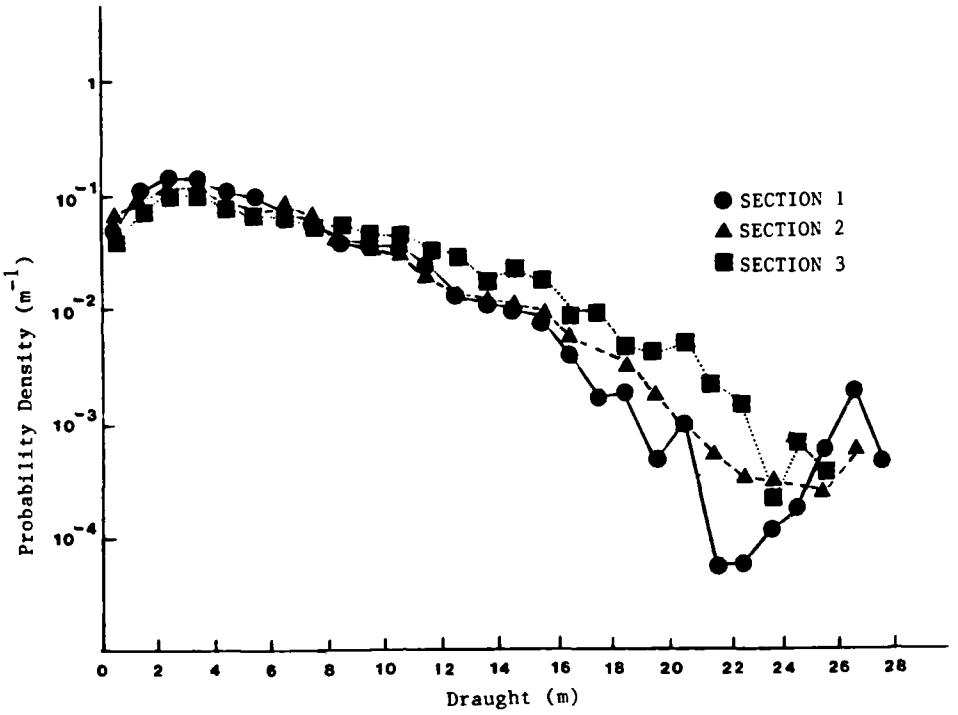

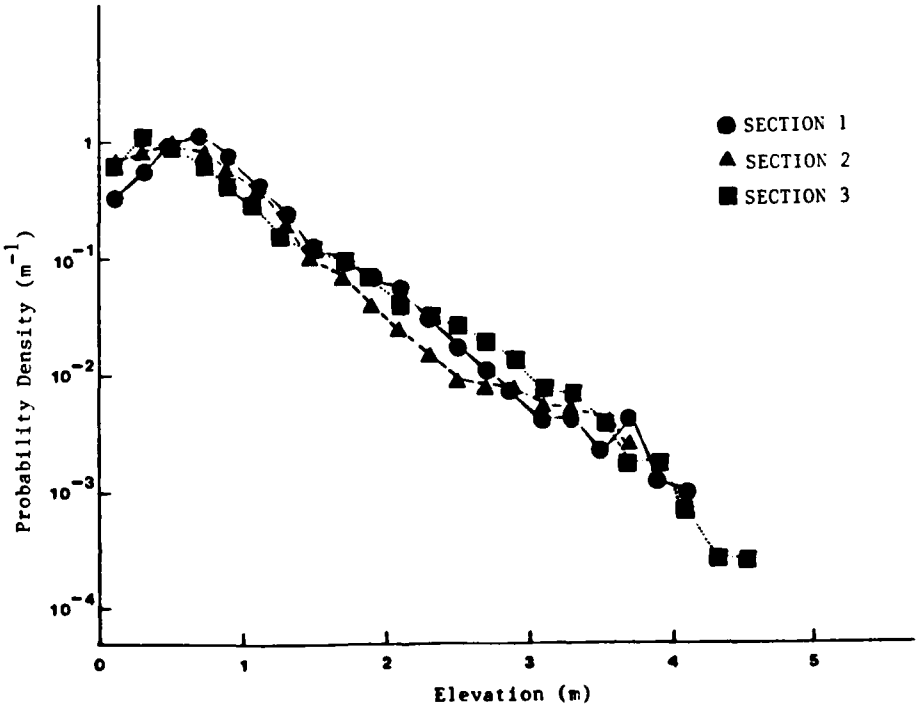

Figure 3. Distributions of the draught and elevations from 20km sections.

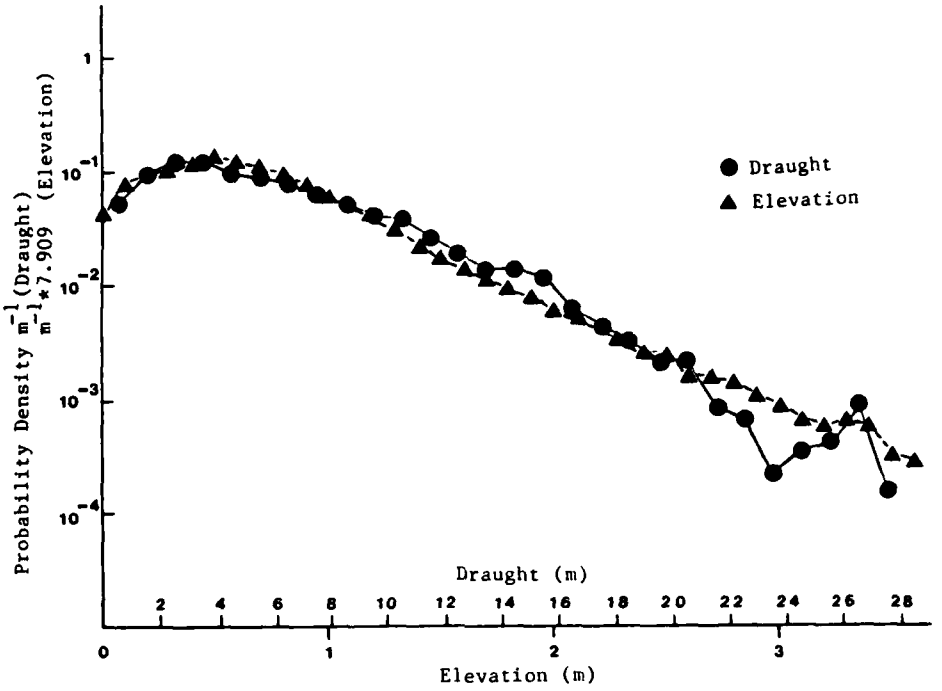

Figure 4. Results of a coordinate transformation in which the elevation distribution for 60km of track is stretched along the abscissa by a factor of 7.909 (mean draught / elevation ratio) and plotted against the corresponding draught distribution.

Thus, we conclude that, in ice cover typical of the central Arctic, it is possible to derive the probability density function of ice draught (and thus of ice thickness) solely from the results of airborne laser profiling. This result has important implications. Since airborne surveys are easier to conduct than submarine surveys, it greatly enhances our ability to monitor synoptically the ice thickness distribution in the Arctic in order to test for evidence of thinning in response to greenhouse warming.

Work is in progress to check this result by comparisons of longer sections of data from other parts of the Arctic.

An analysis was also carried out of ridge and keel distributions. Figure 5 shows the three pairs of ridge elevation and draught distributions. All are approximately negative exponentials. By combining the Sections 1, 2 and 3 and comparing the best fit negative exponentials, we found that an empirical transformation could be carried out to derive keel distributions from sail distributions. However, these transformations are not based on isostasy, as before. Each distribution takes the form:

$$n(h)\ dh = A\ e^{(-ah)}\ dh \qquad (2)$$

where n(h) is the number density of ridges per unit distance and unit height increment, and A, a are parameters characteristic of the ice regime. If we use subscripts $_t$ and $_b$ for top and bottom surfaces, then it was found that the use of the ratios $a_b/a_t = 6.3$; $A_b/A_t = 9.0$, allows a keel distribution to be obtained from a sail distribution. Once again, this requires testing using longer sections of data before it can be applied generally.

These results are discussed fully in Comiso et al. (1989).

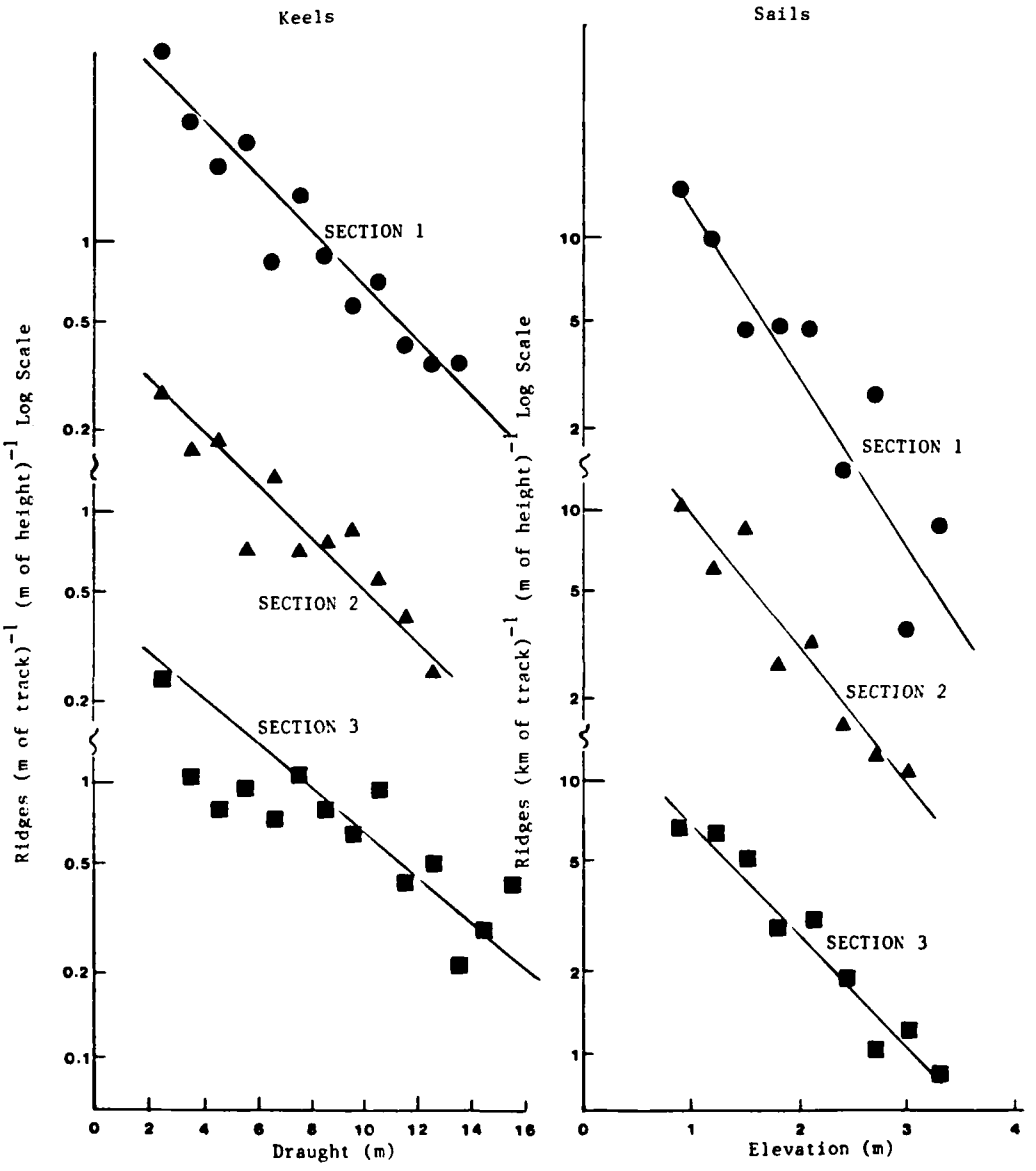

Figure 5. Distributions of keel draught and sail elevations for a 20km section.

5. SONAR/LASER/SAR COMPARISONS

As part of the intensive analysis reported in Wadhams et al. (1989), we used sections 10 and 22km in length to compare SAR brightness with respect to ice draught and ice elevation. results are fully described in Wadhams et al. (1989), which is enclosed in Appendix 4. A brief summary follows.

The original SAR pixels (15.45m x 5.6m) were subsampled 1 by 3 in order to obtain pixels covering an area of 15.45m x 16.8m (16.8m along track). The sonar and laser data were filtered to have equivalent along track resolutions. Point-for-point comparisons were then made of SAR brightness (on an uncalibrated linear scale of 0 to 255) and ice draught or elevation. It was found that the residuals of linear regressions between SAR and laser and between SAR and sonar data were not normally distributed. Therefore,to obtain valid regression analyses it was necessary to transform to square roots for SAR versus sonar,and to square root (SAR) versus fourth root (laser). For the shorter dataset it was found that the variances explained in transformed laser height and sonar depth by transformed SAR brightness were 15.8% and 17.1% respectively.

The results were promising enough to justify a comparison for ice draught over the longer stretch of track, which would also allow us to determine an averaging length for SAR brightness and ice draught which would give the best and most useful correlation. It was found that using a 22km section required further speed adjustments in order to obtain a good SAR/sonar match and that it was not then necessary to use a square root transformation of the data. The resulting correlation coefficient for point-to-point comparison of sonar and SAR was 0.39. Both SAR and ice draught were then windowed over n pixels (i.e. along track distance of 16.8m) to try to improve the correlation.

The correlation coefficient r for SAR brightness versus ice draught increased with n, but there is an upper useful limit dictated by the need to have a good spread of data in the scatter diagrams rather than closely clustered average ice data. We found that n = 15 gave the most useful and meaningful windowed correlation, with an r of 0.68. This implies that 46% of the variance in ice draught can be explained in terms of SAR brightness variations. The

corresponding averaging length is 252m, which is less than that required for the autocorrelation function of the ice bottom to go to zero, i.e. each windowed data point corresponds to a reasonably coherent ice regime rather than averaged conditions.

The high correlation gives some promise that X-band SAR can be used as an empirical means of inferring ice draught distribution, or at least of inferring mean ice draught within a region. However,the correlation can never be as good as that between sonar and laser, since ice elevation and draught are connected (however indirectly) by isostasy, whereas SAR brightness is determined by ice roughness, salt content and snow cover and is only fortuitously related to ice draught.

6. SONAR/PASSIVE MICROWAVE COMPARISONS

The combination of platforms provides a unique opportunity for the validation of passive microwave data over long lengths of track. Our initial analysis compared AMMR with ice type and ice draught. The whole intensively co-registered track, some 190km in length, was used as the test region. AMMR footprints were marked in their correct positions on the SAR image matrix on the *SAIC GEMS* system, using information supplied by NASA. Each footprint, when the P-3A was flown at low level, is an ellipse of along track length 33m and breadth 50m (to 3dB points). The footprints were then transferred manually to a photomosaic of the sidescan sonar imagery, and the following analyses carried out:-

i) Dominant and subsidiary ice type within the footprint were determined by inspection of the sidescan image in conjunction with the SAR image. Ice was classified as ridged; undeformed multiyear; undeformed firstyear; young ice; refrozen lead; and open lead.

ii) Wherever the footprint overlapped the submarine track itself, the ice draught was measured from the 780 upward-looking sonar and given as an average for the 33m length of the footprint.

Some 280 footprints were analysed, of which 40 yielded ice draughts as well as types. J. Comiso then used these results in conjunction with passive microwave brightness temperatures to see if each ice type gave a meaningful cluster in a multifrequency analysis. Results are reported in Comiso **et al.** (1989). Generally it was found that the large amount of deformed ice in this region hampered ice discrimination, but some useful conclusions could still be drawn.

7. SAR DATA ANALYSIS

An investigation was carried out on the SAR pixel frequency distribution for the various ice types within the ONR SAR image. The high Arctic multiyear ice could be separated visually into six distinct ice types. These were: lead; new ice; firstyear (FYR) ice; smooth floes; complex floes and ridges. Ice types within the above categories were confirmed by visual comparison of the SAR image with the sidescan data.

The aim of the investigation was to determine whether different ice types within a SAR image of multiyear ice could be distinguished automatically using a digital thresholding procedure. First, the six ice categories were identified as training areas on the SAR image using the GEMS image processing system at SAIC. Initially, training areas on the SAR image were selected from along the submarine track. This enabled direct comparison of ice types with the baseline sidescan data. Once the ice types for the training areas were confirmed, samples were taken across the entire image using SAR temperature brightness values and texture to verify decisions made based on visual interpretation. For each ice type, several regions were selected for analysis within the study zone. As far as possible, the training areas were of a similar size so that they could be statistically comparable.

Second, pixel values were extracted from the SAR image for all the regions within the individual classes. Then the brightness values for each class were normalised and plotted as frequency histograms showing the pixel distribution for each ice category (Figure 6a to f). The pixel frequency distributions for the six classes were plotted on one graph (shown in Figure 7). Finally, for each class basic statistics were calculated, including the mean, maximum and minimum pixel values, standard deviation and variance (Table 1).

The overlapping pixel frequency distributions for the six ice categories are clearly shown by Figure 7. Although they could be separated visually relatively easily, using tonal and texture information, the digital separation of the SAR pixel brightness distributions was too small. Thus, four

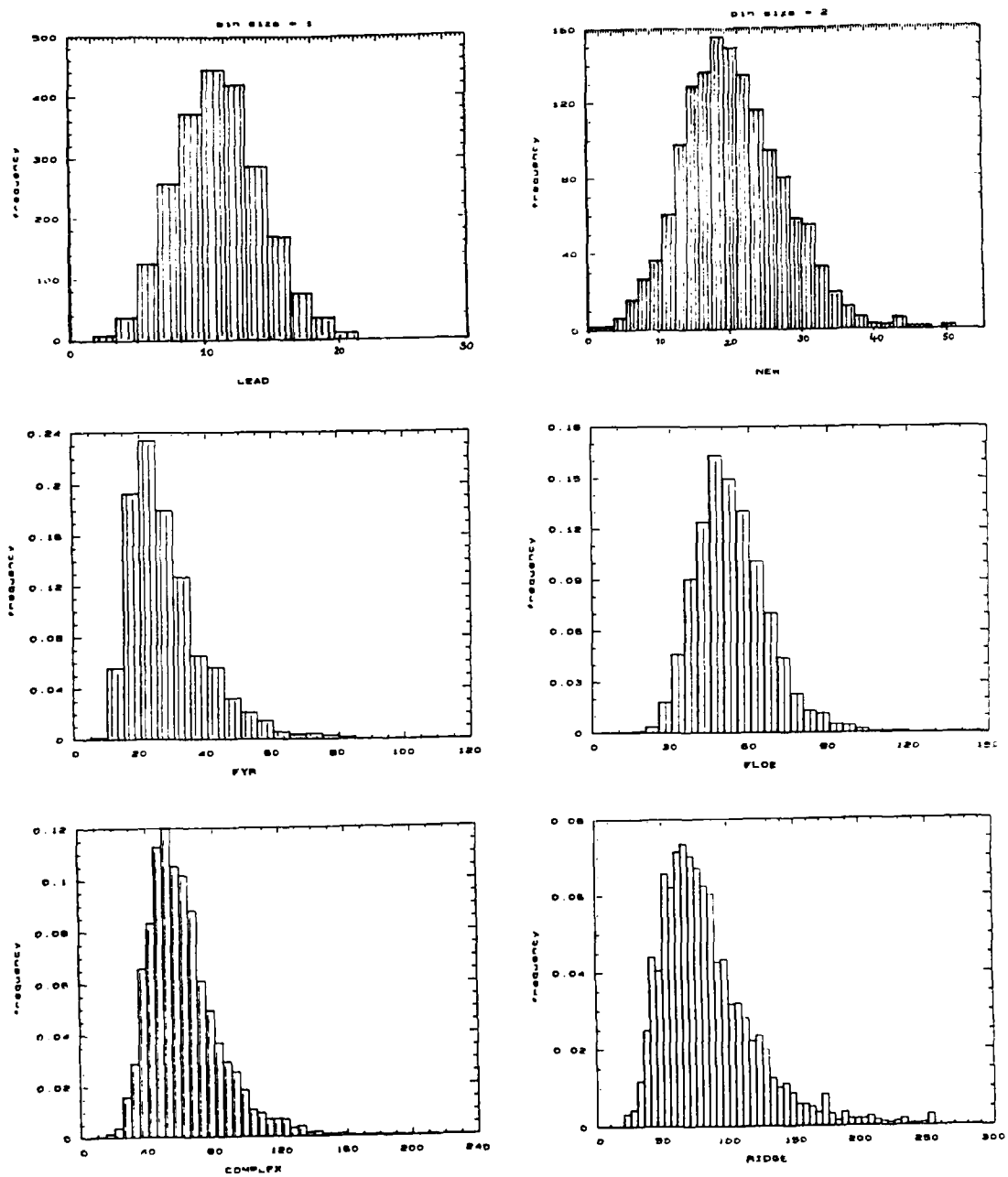

Figure 6: Histograms showing the SAR pixel frequency distribution for the following ice types: (a) lead; (b) new; (c) FYR ice; (d) floe; (e) complex MYR ice and (e) ridges.

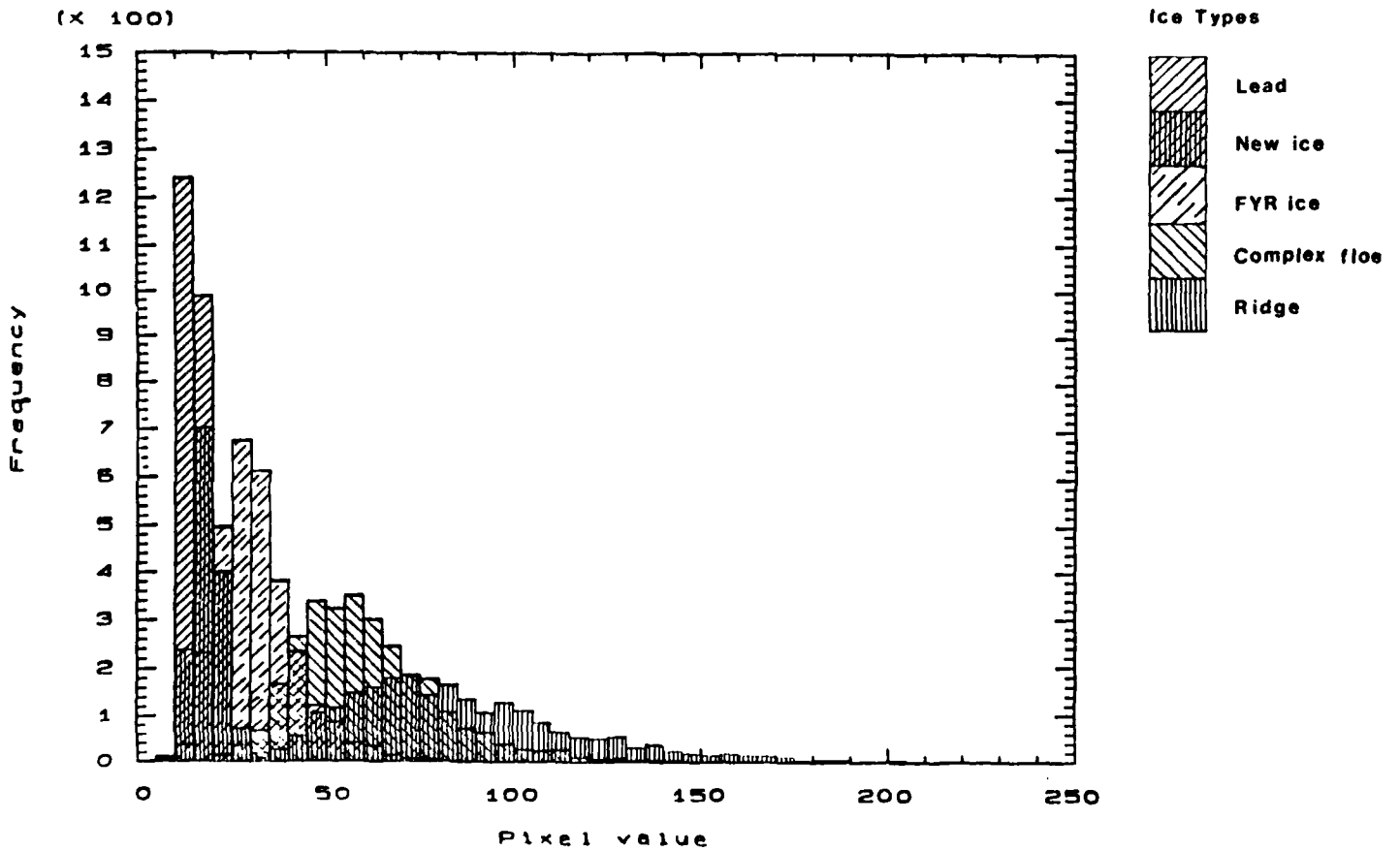

Figure 7. Histograms of SAR pixel frequency for five ice types based on training area analysis.

broader classes were defined. These were: lead and new ice; FYR ice; floe and complex floe (or multiyear ice, MYR) and ridges. these classes can be successfully separated digitally.

Investigation of class statistics can provide digital data on the textural properties of the ice types. Application of a simple maximum likelihood classification procedure, using the GEMS image analysis system, proved relatively successful, at least visually. Further investigation is required to develop more complex classification procedures for distinguishing ice types.

Variable		Lead	New	FYR
Sample size	602	279	1450	
Mean		15.6	18.7	28.6
Median		15.5	18	26
Mode		15	18	21
Standard deviation	2.1	4.5	11.6	
Standard error		0.1	0.3	0.3
Minimum		8	7	9
Maximum		23	40	110
Skewness		0.2	1.2	1.5

Variable		Complex	Floe	Ridge
Sample size	3106	3942	2818	
Mean		62.4	53.6	84.8
Median		59	52	77
Mode		62	49	72
Standard deviation	21.5	13.8	36.0	
Standard error		0.4	0.2	0.7
Minimum		18	20	21
Maximum		214	150	254
Skewness		1.4	0.9	1.5

Table 1. Basic Statistics for the following training areas: lead; new ice; FYR ice; complex MYR ice; smooth floes and ridges.

8. PROGRAMME STATUS

At the time of compiling this interim project report, the following points can be made in respect of progress.

During Phase 3 the major effort has been the processing and intercomparison of several data sets which were collected on May 20th 1987.

The final report on the analysis of the 1987 data, which will be a revised version of this report, will be submitted in December 1989.

The list of Phase 3 tasks in the contract scope of work was refined by the technical participants in the Cambridge Workshop of November 1988 and in the Wallops Workshop of March 1989 (see Appendices 1 and 2). These Phase 3 tasks were aimed at the production of several scientific papers and can be catagorised thus:

I. All analyses for and preparation of a 'Science Paper'[1]

II. All analyses for and preparation of a 'JGR Paper'[2]

III. Future analyses, not specifically related to, or required for, the papers listed above but which could lead to further publications.

IV. Another deliverable, not presaged, was Wadhams and Martin (1989), a CRREL report.

The status of these various tasks are as follows:

I. 'Science Paper' - 100% complete

Individual tasks required to prepare the paper are not listed in Appendices 2 or 3. The paper recently submitted to EOS, satisfies the project requirements as outlined in the two workshop proceedings.

---

[1] Wadhams **et al.** (1989), now submitted to EOS and included in Appendix 4.

[2] Prepared for submission to JGR.

II. 'JGR Paper' - 100% complete (awaiting submission)

The JGR paper has been written and prepared for submission for publication.

The five data analysis stages listed in Item 5 of the Cambridge Workshop proceedings were revised during the NASA Wallops Workshop. Item 6 of the proceedings has been accomplished by SAIC Cambridge.

Further tasks are listed in the Cambridge workshop proceedings, under the heading 'Understanding on processing of data from the 1987 experiment'. It is the understanding of SAIC Cambridge that all tasks listed in Paragraphs 1 to 4 have been completed.

Seven specific data analysis tasks were allocated to team members during the NASA Wallops workshop (see Appendix 2). All tasks allocated to SAIC Cambridge have been completed.

In conclusion, the JGR paper is now written and was due to be submitted at the end of August or beginning of September.

III. Future Tasks

Future tasks, which may be allocated to Phase 4, are outlined in the NASA Wallops proceedings under the heading '3. Future Tasks'.

9. PHASE 4 WORK TO BE ACCOMPLISHED

The major aims of 1987 data analysis to be completed in Phase 4, are:

1. To choose another region for intensive analysis and replicate the direct sensor comparisons discussed here and presented in Wadhams **et al.** (1989) and Comiso **et al.** (1989). The probable choice will be a region further to the east, in the vicinity of 84°N 10°W.

2. To complete the statistical analysis of ULS data for the first part of the voyage and publish an interpretation of the complete dataset.

3. To publish an interpretation of the wave number spectra results.

4. To extend the sonar-laser comparison to longer stretches of data (to be done in collaboration with Tucker, Swift and Krabill).

10. REFERENCES

** A paper written on Phase 2 of the contract
*** A paper written during Phase 3 of the contract

Bass, F.G.and I.M. Fuks (1979). Wave scattering from statistically rough surfaces. Pergamon,New York.

***** Comiso, J.C., P. Wadhams, W. Krabill, R. Swift, J. Crawford and W. Tucker (1989).** Top/bottom multisensor remote sensing of Arctic sea ice. J. Geophys. Res., in preparation (to be submitted 31 Aug. 1989).

**** Guoliang, J. and P. Wadhams (1989).** Travel time changes induced in a tomography array caused by a sea ice cover. Progress in Oceanogr. in press.

Lowry, R.T. and P. Wadhams (1979). On the statistical distribution of pressure ridges in sea ice. J.Geophys.Res., 84, 2487-2494.

Lysanov, Yu.P. (1974). Scattering of sound by rough surface. In Ocean Acoustics, (L.M. Brekhovskikh, ed.), Nauka, Moscow.

Wadhams, P. (1978). Characteristics of deep pressure ridges in the Arctic Ocean. Proc. 4th Intl. Conf.on Port and Ocean Engng Under Arctic Conditions, St. John's (ed. D.B. Muggeridge), Memorial Univ., St. John's, Nfld., 1, 544-555.

Wadhams, P. (1981). Sea-ice topography of the Arctic Ocean in the region 70°W to 25°E. Phil. Trans. Roy. Soc., Lond., 302A., 45-85.

Wadhams, P. (1983). The sea ice thickness distribution in Fram Strait. Nature, Lond., 305, 108-111.

**** Wadhams, P. (1988).** The underside of Arctic sea ice imaged by sidescan sonar. Nature, Lond., 333, 161-164.

***** Wadhams, P., J.C. Comiso, A.M. Cowan, J. Crawford,G. Jackson, W. Krabill, R. Kutz, C.B. Sear, R. Swift and W.B. Tucker (1989).** Concurrent remote sensing of Arctic sea ice from submarine and aircraft. EOS, Trans. Am Geophys Union, submitted (enclosed with this report).

Wadhams, P. and T. Davy (1986). The distribution of pressure ridge depths and spacings in sea ice. J. Geophys. Res., 91, 10697-10708.

***** Wadhams, P. and S. Martin (1989).** Processes determining the bottom topography of multiyear Arctic sea ice. US Army Cold Regions Res. & Engng. Lab., Hanover, NH., Special Rept. W.F. Weeks Volume, in press (enclosed with this report).

11. ACKNOWLEDGEMENTS

This report was written primarily by Dr. P. Wadhams, with some material from Ms. A Scoon. The report was compiled, edited and produced by Dr. C Sear, S Moore and D Evans at SAIC in Cambridge.

The work described and carried out by SAIC in Cambridge was undertaken by Drs. Wadhams and Sear, S Moore, Ms. A Scoon and N Flack.

At SAIC Cambridge, adminstrative support was given by Ms. M Cowan and managerial support by A Cowan.

APPENDIX 1

Proceedings of the data workshop held in Cambridge
November 1988

PROCEEDINGS OF SUBMARINE/AIRCRAFT DATA WORKSHOP, CAMBRIDGE, 8-10 NOV 1988

1. A workshop was held at Scott Polar Research Institute (SPRI) and Polar Oceans Associates (POA), Cambridge, from 8-10 November 1988 to finalise the text of a paper for "Science" omn the results of the 1987 submarine/aircraft experiment, and to plan further stages of data processing.

2. Attendees were

Miss K Baird	Admiralty Research Establishment (ARE)
Mr J Carter	ARE
Dr J C Comiso	NASA Goddard
Mr A M Cowan	POA
Dr J Crawford	Jet Propulsion Laboratory (JPL)
Dr B Hughes	ARE
Dr G Jackson	ARE
Dr W Krabill	NASA Wallops
Dr R Swift	NASA Wallops
Dr R H Thomas	NASA Headquarters
Dr P Wadhams	POA and SPRI

3. An understanding was reached on the use and release of data with respect to possible security sensitivities. The text is enclosed. This has been sent to Cdr Weeks at Fleet Headquarters, FOS/M, Northwood, for his agreement.

4. A set of figures and an almost-final text of the "Science" paper were determined. These will be circulated by mail. It was decided that final sections of imagery and profile for the three figures should be sent to Comiso as quickly as possible, and final text addenda to Wadhams as quickly as possible.

5. Ongoing collaboration to produce a paper for JGR and further papers depends on using the SAR imagery as a matrix for co-registering both aircraft tracks and the submarine track. The next stages of this will be as follows:
a) JPL sends Wallops a registered SAR image (in the form of two tapes, one with raw pixels, one with square pixels) of the entire May 20 track for providing a common frame of reference for all investigators. It will be 12450 records in length by 2200 bytes wide, at 6250 BPI, with no label and no blocking.
b) Wallops will add lat-long information in Intel floating point 64 bit format, for the left and right hand sides of each record. A subroutine will be added to the tape such that a user can enter lat-long data and get a row and pixel number to find the spot on the image.
c) Wallops will also add AOL and PRT-5 data in the format SAR row no (raw): SAR row no (square): lat in deg/min/s x 100: long in deg/min/s x 100: elevation in m x 100: temp x 100.
d) Wallops sends to POA. POA adds similar dataset to (c) for ice draft from submarine data.
e) POA sends to all investigators.

6. The sub track will be located on the SAR by matching features found on the side scan sonar records recorded by the sub. This matching is possible because the time difference between the imaging of the ice by side scan and the SAR is small (at the most 2 hours). The latitudes and longitudes of the track can then be computed given that the coordinates of the first pixel on each line is known and that the pixel size of the SAR is known. The aircraft track will be marked directly on to the geolocated SAR image using the coordinate information recorded during the flight.

The completed tape will be sent out to all investigators in the group.

Nothing round.

7. Provisional date for submission is end of the year. The next data workshop will be held in Wallops, provisionally in March 1989. Wadhams, Swift and Comiso will try to meet at AGU Fall Meeting.

UNDERSTANDING ON PROCESSING OF DATA FROM 1987 EXPERIMENT

A workshop was held in Cambridge on 8-10 November 1988 involving the following persons who form the analysis team for the data from the 1987 submarine-aircraft joint remote sensing experiment:- Dr P Wadhams - SPRI, Polar Oceans Associates
Mr A M Cowan - Polar Oceans Associates
Dr G Jackson, Dr B Hughes, Mr J Carter, Miss K Baird - Admiralty Research Establishment
Dr J C Comiso - NASA Goddard
Dr W Krabill, Dr R Swift - NASA Wallops
Dr J Crawford - JPL
Dr R H Thomas - NASA Headquarters
The following understanding was reached about the way in which the team would like to analyse and publish results from the experiment. We seek the guidance and written approval of FOS/M for these plans.

1. Current analysis of the 20 May 1987 SAR, sonar, laser and microwave data sets have led to the potential development of several scientific papers. These papers will describe broad relationships between observations acquired with these various sensors, and relationships between these data sets and satellite imagery.

2. In order to allow reasonable comparison between these relationships and previously reported historical ice data, we seek to report the approximate location and time of the 20 May observations in the following way. The flight/submarine locations in the region of 35oW - 15oW at 85oN would be shown in the form of a box drawn on a large-scale map such that the track or location cannot be inferred to better than 50 km accuracy. The timing of the observations is, however, felt to be more critical since at this time of year ice conditions change rapidly in the Arctic (transition into spring). Further, this date has already been reported in a paper. We therefore seek to use this date so that we may also make use of concurrent satellite imagery in the paper.

3. During analysis and comparison of the sonar versus aircraft datasets for 19-25 May it is necessary to co-register the submarine and aircraft tracks. We intend to do this as follows:-

a) The submarine navigation data will remain with P. Wadhams and will be treated as Secret UK/US Eyes Only.
b) The submarine track will be co-registered with (i.e. overlaid on) the SAR imagery purely for the purposes of analytical work, as will the tracks of the aircraft. This will be used to produce a common imagery data set expressed in arbitrary co-ordinates (not latitude and longitude) for use by the various scientists in the project.

4. Draft texts of all papers arising from this project which pertain to the submarine will be submitted to FOS/M for approval. The first papers to appear will be oral and poster presentations at the American Geophysical Union meeting in San Francisco in December. Three papers will be given. Two will discuss only the airborne aspects of the 20 May experiment and will not discuss submarine results. The third will discuss ice growth mechanisms and will make use of two sidescan images of ice already published in "Nature", without saying anything about time or location of collection. A copy of the abstracts of these papers will be sent to you next week.

5. Dr J Crawford will be provided with a stretch of sidescan sonar data, with no information on location, for the purpose of developing a three-dimensional simulation of the image for animation purposes.

6. Based on telephone discussions between Cdr Weeks of FOS/M and Dr Thomas of NASA on 9 November we understand that, two years after data acquisition (i.e. in May 1989) a set of the May 1987 sonar data, including navigation information, will be released for archival and open distribution to other investigators.

7. We propose that these procedures be adopted in analysis of future sets of submarine data that are apporoved for limited release by FOS/M.

APPENDIX 2

Proceedings of the project meeting held at NASA Wallops
March 1989

PROCEEDINGS OF MEETING ON SUBMARINE/AIRCRAFT PROJECT
NASA Wallops, 27-28 March 1989

Attendees:-

Peter Wadhams	SAIC - Polar Oceans Associates
Joey C Comiso	NASA Goddard
Bill Krabill	NASA Wallops
Bob Swift	NASA Wallops / EG & G
Terry Tucker	CRREL
John P Crawford	JPL.

The meeting was concerned with three main issues:
-completion of the "Science" paper
-analysis and writing plans for "JGR" paper
-plans for further analysis of remaining data.
All issues were resolved successfully, as follows.

1. Science paper

The text for the paper was completed. The most recent analytical work which led to the completion of the main text and fig. 3 was the cross-correlation analysis of SAR brightness versus AOL elevation. It was found that the fourth root of the AOL elevation versus the square root of the SAR brightness (necessary to yield pdfs with normal residuals) gave a linear regression with a correlation coefficient of 0.4 on a point-to-point comparison. A similar correlation had already been obtained for sonar ice draft (sqrt) versus SAR brightness (sq rt). This gave considerable promise as a potential tool for inferring mean ice thickness or even ice thickness distribution from SAR brightnesses. But further work is necessary using longer pieces of data for the comparisons, rather than a single point where a small error in registration could throw off the correlation. This was identified as a task for the JGR paper. Further material was added on passive microwave and other sections. The following action items remain to be completed within the next week:-

1. Write summary - PW
2. Add paragraph on PRT5 interpretation - JCC
3. Show draft to "Science" - PW and JCC, March 30
4. Complete artwork on figures - JCC
5. Show to FOS/M - PW
6. Reference on ice drilling - WBT.

Submission date 9 April. (Note: Tasks 1,2,3 are accomplished on 3/30/89

2. JGR paper

The scope of work and contents of this paper were agreed on, and a provisional completion date of June decided upon. JCC provided a working text of the introductory part of the paper, with suitable illustrations, and the following tasks and action items were agreed for the data analysis which still remains to be done.

Task 1. Use the sidescan to identify areas occupied unequivocally by ice of a single type - undeformed multiyear, undeformed first-year (definitely), deformed multiyear, young ice, open water (possibly) - in regions which fall within the low-level AMMR footprint. Use this identification to obtain a set of multifrequency brightness temperatures

for definitely validated ice types (where the area crosses the actual submarine track this validation also includes draft). In this way examine the real variability of passive microwave over ice of a well defined type. Action. Basic dataset for this and other tasks is 190 km track from 20 May. PW places submarine track on square pixel-averaged SAR image which already contains laser track. Sends co-ordinates of this to WK/RS as DOS disk by end of next week. WK plots centre of footprint of each AMMR reading on this image, sends to PW. PW examines each footprint where it falls within sidescan swath, determines whether whole area is covered by a unique ice type or a mixture. Produces a log of ice type versus AMMR record number, sends to JCC, JPC. JCC retrieves brightness temperatures, produces cluster diagrams of Tb versus ice type, interprets meaning.

Task 2. Continue and extend the AOL/SAR and sonar/SAR cross-correlations, using the entire 100 km (sonar/SAR) or 190 km (AOL/SAR) and trying different averaging lengths and statistical techniques in an attempt to increase the degree of correlation to a level which is genuinely useful as a tool in ice thickness inference. Action. PW to do the sonar/SAR comparisons, WBT to do the AOL/SAR comparisons, with both teams keeping in close contact.

Task 3. Compare statistics of ice draft obtained from upward sonar with corresponding statistics of elevation obtained from laser. Action. PW showed statistics obtained from 50 km sections of sonar data. He passed these to WBT for guidance. The statistics comprise line printer tabulations and graphical outputs on pdf of ice draft, distributions of smooth and rough ice drafts, pressure ridge draft and spacing distributions, lead width/spacing/ice thickness distributions, floe width distributions etc. WBT is generating similar statistics for upper surface. WBT will send PW co-ordinates of start/end points of 20 km sections, which is basis for his statistics. PW will redo submarine statistics for same 20 km sections. Both teams will keep in close touch on joint interpretation. PW passed the relevant 100 km of corrected, interpolated upward sonar data to WK.

Task 4. Compare mean SAR backscatter with 37 GHz AMMR horizontal brightness temperatures. Visually there appear to be episodes of strong negative correlation, interspersed with periods of no apparent correlation. Develop suitable statistics to deal with this and interpret. Action. JCC and JPC to do.

Task 5. Carry out a cluster analysis which includes SAR brightness as well as AMMR brightneses. Action. JCC and JPC to do.

Task 6. For a few clear cases only, compare real lead widths as seen from sidescan and SAR with visibility of same leads on AVHRR. Display on fig. 2 of paper. Action. JCC and PW to do. Develop this further as larger task for future paper.

Task 7. Combine PRT5 data with AMMR brightness temperature data to infer emissivity. Use emissivity for pdfs of AMMR. Action. JCC to do.

3. Future tasks

a) Extend tasks 1-5, 7 to entire dataset, 19-21 May (although AOL data not

good on 19th). PW has already computed sonar statistics for entire 3400 km of submarine track in 50 km sections. For other correlations, 21st appears to be best dataset.(All teams)
b) Carry out systematic study of task 6 to define minimum lead width which is definable on AVHRR.(PW, JCC)
c) Carry out pattern recognition and expert system analyses of SAR (JPC)
d) Do comparison of statistics from large-scale (high-level) AMMR with sonar statistics on 50 km scale length (JCC, PW).

APPENDIX 3

Sea ice draught distribution statistics
for a sample 50km section (Section 1)

****

SEA ICE DRAFT STATISTICAL PARAMETERS

****

3.700	SEA ICE DRAFT - MODAL VALUE
4.51692	SEA ICE DRAFT - MEAN VALUE
5.14727	SEA ICE DRAFT - RMS VALUE
17.21597	SEA ICE DRAFT - VARIANCE
4.14697	SEA ICE DRAFT - STANDARD DEVIATION
3.93892	SEA ICE DRAFT - MEDIAN VALUE

****

STATISTICAL PARAMETERS EXERCISING NEGATIVE POINTS

****

4.94375	SEA ICE DRAFT - MEAN VALUE
5.17.64	SEA ICE DRAFT - RMS VALUE
17.13669	SEA ICE DRAFT - VARIANCE
4.14632	SEA ICE DRAFT - STANDARD DEVIATION
3.93892	SEA ICE DRAFT - MEDIAN VALUE

POLYNYA/LEAD DISTRIBUTION - 50 KM SECTION
OCCURANCE OF LEADS/POLYNYA IN RANGES AND
CONDITIONAL PROBABILITY OF RANGES

NUMBER OF LEADS/POLYNYA (1000 POINTS) PER RANGE — NUMBER OF LEADS/POLYNYA IN SECTION (UNCORRECTED)

MINIMUM DRAFT RANGE(M)	0.5M	0.75M	1.0M	0.5M	0.75M	1.0M
> 0	[illegible]	231.7[illegible]	275.[illegible]	[illegible]	37.[illegible]	[illegible]
> 10	4[illegible].24631	4[illegible]	77.[illegible]77	12.0	14.0	[illegible]
> 20	20.12341	25.[illegible]121	36.[illegible]	6.0	[illegible]	11.0
> 30	16.75352	20.13510	20.12341	5.0	[illegible]	6.0
> 40	6.70731	10.06171	10.06171	2.0	3.0	3.0
> 50	3.35390	10.06171	16.75352	1.0	3.0	5.0
> 60	15.75352	13.41561	15.76352	5.0	4.0	5.0
> 70	13.41561	3.35390	10.06171	4.0	1.0	3.0
> 80	0.00000	3.35390	3.35390	0.0	1.0	1.0
> 90	0.00000	3.35390	0.00000	0.0	1.0	0.0
> 100	3.35390	10.06171	15.75352	1.0	3.0	5.0
> 120	0.00000	0.00000	6.70731	0.0	0.0	2.0
> 140	0.00000	0.00000	0.00000	0.0	0.0	0.0
> 160	0.00000	3.35390	0.00000	0.0	1.0	1.0
> 180	0.00000	0.00000	0.00000	0.0	0.0	0.0
> 200	0.00000	0.00000	3.35390	0.0	0.0	1.0
> 250	3.35390	0.00000	0.00000	1.0	0.0	0.0
> 300	0.00000	0.00000	0.00000	0.0	0.0	0.0
> 350	0.00000	6.70731	3.35390	0.0	2.0	1.0
> 400	0.00000	0.00000	0.00000	0.0	0.0	0.0
> 450	0.00000	0.00000	0.00000	0.0	0.0	0.0
> 500	0.00000	0.00000	3.35390	0.0	0.0	1.0
> 550	0.00000	0.00000	0.00000	0.0	0.0	0.0
> 600	0.00000	0.00000	0.00000	0.0	0.0	0.0
> 650	0.00000	0.00000	0.00000	0.0	0.0	0.0
> 700	0.00000	0.00000	0.00000	0.0	0.0	0.0
> 750	0.00000	0.00000	0.00000	0.0	0.0	0.0
> 800	0.00000	0.00000	0.00000	0.0	0.0	0.0
> 850	0.00000	0.00000	0.00000	0.0	0.0	0.0
> 900	0.00000	0.00000	0.00000	0.0	0.0	0.0
> 950	0.00000	0.00000	0.00000	0.0	0.0	0.0
> 1000	3.35390	3.35390	3.35390	1.0	1.0	1.0

LEAD/POLYNYA ANALYSIS STATISTICAL PARAMETERS

MINIMUM DEPTH DRAFT 0.5 METRES

396.74[illegible] LEAD/POLYNYA ANALYSIS - NUMBER/100 KM

3.35760 LEAD/POLYNYA ANALYSIS - NUMBER/KM

25.21356 LEAD/POLYNYA ANALYSIS - MEAN VALUE

404.39136 LEAD/POLYNYA ANALYSIS - RMS VALUE

9559.23.47 LEAD/POLYNYA ANALYSIS - VARIANCE

97.77960 LEAD/POLYNYA ANALYSIS - STANDARD DEVIATION

7.00000 LEAD/POLYNYA ANALYSIS - MEDIAN VALUE

STATISTICAL PARAMETERS EXCISING NEGATIVE POINTS

25.21356 LEAD/POLYNYA ANALYSIS - MEAN VALUE

101.53136 LEAD/POLYNYA ANALYSIS - RMS VALUE

5196.39042 LEAD/POLYNYA ANALYSIS - VARIANCE

96.49141 LEAD/POLYNYA ANALYSIS - STANDARD DEVIATION

7.00000 LEAD/POLYNYA ANALYSIS - MEDIAN VALUE

MINIMUM DEPTH DRAFT 0.75 METRES

4e2.83361 LEAD/POLYNYA ANALYSIS - NUMBER/100 KM

3.61781 LEAD/POLYNYA ANALYSIS - NUMBER/KM

31.62751 LEAD/POLYNYA ANALYSIS - MEAN VALUE

103.0736[illegible] LEAD/POLYNYA ANALYSIS - RMS VALUE

9924.[illegible]34 LEAD/POLYNYA ANALYSIS - VARIANCE

99.61243 LEAD/POLYNYA ANALYSIS - STANDARD DEVIATION

7.00000 LEAD/POLYNYA ANALYSIS - MEDIAN VALUE

STATISTICAL PARAMETERS EXCISING NEGATIVE POINTS

31.62751 LEAD/POLYNYA ANALYSIS - MEAN VALUE

103.[illegible] LEAD/POLYNYA ANALYSIS - RMS VALUE

```
      9922.95911  LEAD/POLYNYA ANALYSIS - VARIANCE
        99.61421  LEAD/POLYNYA ANALYSIS - STANDARD DEVIATION
         7.00000  LEAD/POLYNYA ANALYSIS - MEDIAN VALUE
**********************************************************************

    MINIMUM DEPTH DRAFT 1.0 METRES
**********************************************************************
       535.42945  LEAD/POLYNYA ANALYSIS - NUMBER/100 KM
         5.35439  LEAD/POLYNYA ANALYSIS - NUMBER/KM
        35.84335  LEAD/POLYNYA ANALYSIS - MEAN VALUE
       135.40939  LEAD/POLYNYA ANALYSIS - RMS VALUE
     10126.51170  LEAD/POLYNYA ANALYSIS - VARIANCE
       100.63057  LEAD/POLYNYA ANALYSIS - STANDARD DEVIATION
         9.00000  LEAD/POLYNYA ANALYSIS - MEDIAN VALUE
**********************************************************************

    STATISTICAL PARAMETERS EXCLUDING NEGATIVE POINTS
**********************************************************************
        35.84335  LEAD/POLYNYA ANALYSIS - MEAN VALUE
       135.40939  LEAD/POLYNYA ANALYSIS - RMS VALUE
     10126.57510  LEAD/POLYNYA ANALYSIS - VARIANCE
       100.63091  LEAD/POLYNYA ANALYSIS - STANDARD DEVIATION
         9.00000  LEAD/POLYNYA ANALYSIS - MEDIAN VALUE
**********************************************************************
```

CONDITIONAL PROBABILITY OF LEADS/POLYNYA (10/000)

****

RANGE(M)	MINIMUM DRAFT 0.5	0.75	1.0
>	[illegible]	[illegible]	[illegible]
> 10	[illegible]	0.10145	[illegible]
> 20	[illegible]	0.05797	0.27235
> 30	0.04257	0.05522	[illegible]
> 40	0.01595	0.02174	[illegible]
> 50	[illegible]	0.01174	[illegible]
> 60	0.04237	[illegible]	[illegible]
> 70	[illegible]	[illegible]	[illegible]
> 80	[illegible]	[illegible]	[illegible]
> 90	[illegible]	[illegible]	[illegible]
> 100	[illegible]	[illegible]	[illegible]
> 120	[illegible]	[illegible]	[illegible]
> 140	[illegible]	[illegible]	[illegible]
> 150	[illegible]	[illegible]	[illegible]
> 180	[illegible]	[illegible]	[illegible]
> 200	[illegible]	[illegible]	[illegible]
> 250	[illegible]	[illegible]	[illegible]
> 300	[illegible]	[illegible]	[illegible]
> 350	[illegible]	[illegible]	[illegible]
> 400	[illegible]	[illegible]	[illegible]
> 450	[illegible]	[illegible]	[illegible]
> 500	[illegible]	[illegible]	[illegible]
> 550	[illegible]	[illegible]	[illegible]
> 600	[illegible]	[illegible]	[illegible]
> 650	[illegible]	[illegible]	[illegible]
> 700	[illegible]	[illegible]	[illegible]
> 750	[illegible]	[illegible]	[illegible]
> 800	[illegible]	[illegible]	[illegible]
> 850	[illegible]	[illegible]	[illegible]
> 900	[illegible]	[illegible]	[illegible]
> 950	[illegible]	[illegible]	[illegible]
> 1000	[illegible]	[illegible]	[illegible]

LEVEL/ROUGH ICE DISTRIBUTION - 50 KM SECTION

ANALYSIS OF SMOOTH ICE, 50 KM SECTION

27e29.7 NUMBER OF SMOOTH ICE POINTS/100%

27.92 PERCENTAGE SMOOTH ICE

SMOOTH ICE DISTRIBUTION - 50 KM SECTIONS

VALUES CLASSIFIED -1 TO 60 M BY 10 CM DIVISIONS
PROBABILITY DENSITY x 10**4/M, NORMALIZED 100.00
PROBABILITY DENSITY TABLE - 10 CM BINS

METRES	.0+	.1+	.2+	.3+	.4+	.5+	.6+	.7+	.8+	.9+
-1 - 0	62e.67873	73.65876	0.00000	0.00000	122.75963	615.79761	1767.73853	2572.57544	3241.05475	2824.15696
0 - 1	4959.49823	3228.57512	3240.58435	2210.30205	4173.67922	2437.26909	2676.16947	3596.05713	2674.21947	1632.70291
1 - 2	1503.53916	1562.39214	1362.66464	1141.06621	1411.73152	1141.56631	1000.52901	1239.57153	1197.64724	624.76514
2 - 3	341.14509	366.00675	242.96720	65.65508	366.42960	1439.24735	1756.21064	810.21356	1266.14771	1267.18559
3 - 4	1387.15309	1215.32017	1157.12642	949.50102	1339.67203	1045.45679	857.21714	1215.32017	1065.72247	1313.57703
4 - 5	1065.73247	910.21356	1066.00674	773.36500	850.97265	691.07382	471.71404	417.56257	471.76221	242.36662
5 - 6	364.00293	424.21145	364.27511	301.45178	364.89057	147.31164	49.10394	206.66126	110.49360	184.13943
6 - 7	184.12345	73.65876	60.34632	60.29173	122.75963	147.31164	171.84346	17.66346	36.67451	564.68855
7 - 8	728.35742	724.25174	1005.62451	773.36500	270.67104	68.24767	270.67104	135.03567	85.93173	16.87566
8 - 9	24.55101	24.55101	90.20747	0.00000	0.00000	110.49366	0.00000	0.00000	0.00000	0.00000
9 - 10	0.00000	98.20767	24.55191	0.00000	159.59755	196.41535	0.00000	0.00000	0.00000	0.00000
10 - 11	0.00000	0.00000	0.00000	0.00000	0.00000	61.37301	73.65576	24.55101	49.10364	49.10364
11 - 12	0.00000	0.00000	0.00000	0.00000	24.55101	36.82677	12.27588	0.00000	0.00000	196.41567
12 - 13	159.63822	135.03567	49.10364	49.10364	613.79761	196.41535	12.27588	0.00000	0.00000	0.00000
13 - 14	0.00000	0.00000	0.00000	0.00000	73.65576	24.55193	135.03567	220.98243	220.98243	319.17573
14 - 15	0.00000	73.65576	196.41567	0.00000	122.75963	196.41567	49.10364	208.66125	196.41567	147.31164
15 - 16	159.63822	159.63822	61.37301	0.00000	0.00000	0.00000	0.00000	0.00000	0.00000	0.00000
16 - 17	0.00000	0.00000	24.55193	36.82773	0.00000	0.00000	0.00000	0.00000	0.00000	0.00000
17 - 18	0.00000	0.00000	0.00000	0.00000	0.00000	0.00000	0.00000	0.00000	0.00000	0.00000
18 - 19	0.00000	0.00000	0.00000	0.00000	0.00000	0.00000	0.00000	0.00000	0.00000	0.00000
19 - 20	0.00000	0.00000	0.00000	0.00000	0.00000	0.00000	0.00000	0.00000	0.00000	0.00000
20 - 21	0.00000	0.00000	0.00000	0.00000	0.00000	0.00000	0.00000	0.00000	0.00000	0.00000
21 - 22	0.00000	0.00000	0.00000	0.00000	0.00000	0.00000	0.00000	0.00000	0.00000	0.00000
22 - 23	0.00000	0.00000	0.00000	0.00000	0.00000	0.00000	0.00000	0.00000	0.00000	0.00000
23 - 24	0.00000	0.00000	0.00000	0.00000	0.00000	0.00000	0.00000	0.00000	0.00000	0.00000
24 - 25	0.00000	0.00000	0.00000	0.00000	0.00000	0.00000	0.00000	0.00000	0.00000	0.00000
25 - 26	0.00000	0.00000	0.00000	0.00000	0.00000	0.00000	0.00000	0.00000	0.00000	0.00000
26 - 27	0.00000	0.00000	0.00000	0.00000	0.00000	0.00000	0.00000	0.00000	0.00000	0.00000
27 - 28	0.00000	0.00000	0.00000	0.00000	0.00000	0.00000	0.00000	0.00000	0.00000	0.00000

SMOOTH ICE DISTRIBUTION - 50 KM SECTIONS
VALUES CLASSIFIED IN 0.5 & 1.0 M DIVISIONS

PROBABILITY DENSITY TABLE - 50 KM & 1 M BINS

METRES	0.0 - 0.5	0.5 - 1.	1. - 1.5
-1 - 0	822.6	10815.1	11557.
0 - 1	18015.	14619.1	5263.
1 - 2	7.3	772.	1
2 - 3	2576.	6011.	20
3 - 4	5	67.	1137.
4 - 5	424.	1999.	65
5 - 6	1	599.	2
6 - 7	7	1474.	717.
7 - 8	3511.	614.	411.
8 - 9	147.	111.	257.
9 - 10	292.	195.	47.
10 - 11	0	257.	257.
11 - 12	0	542.	824.
12 - 13	16	0	1
13 - 14	0	569.	1065.
14 - 15	1027.	942.	1193.
15 - 16	579.	119.	97.
16 - 17	11.	0	11.
17 - 18	0	0	0
18 - 19	0	0	0
19 - 20	0	0	0
20 - 21	0	0	0
21 - 22	0	0	0
22 - 23	0	0	0
23 - 24	0	0	0
24 - 25	0	0	0
25 - 26	0	0	0
26 - 27	0	0	0
27 - 28	0	0	0
28 - 29	1.	0	1.
29 - 30	0	0	0
30 - 31	0	0	0
31 - 32	0	0	0
32 - 33	0	0	0
33 - 34	0	0	0
34 - 35	0	0	0
35 - 36	0	0	0
36 - 37	0	0	0
37 - 38	0	0	0
38 - 39	0	0	0
39 - 40	0	0	0
40 - 41	0	0	0
41 - 42	0	0	0
42 - 43	0	0	0
43 - 44	0	0	0
44 - 45	0	0	0
45 - 46	0	0	0
46 - 47	0	0	0
47 - 48	0	0	0
48 - 49	0	0	0
49 - 50	0	0	0

****

SMOOTH ICE STATISTICAL PARAMETERS

****

[illegible] SMOOTH ICE DRAFT - MODAL VALUE

2.66297 SMOOTH ICE DRAFT - MEAN VALUE

4.33272 SMOOTH ICE DRAFT - RMS VALUE

11.67403 SMOOTH ICE DRAFT - VARIANCE

3.41673 SMOOTH ICE DRAFT - STANDARD DEVIATION

2.36318 SMOOTH ICE DRAFT - MEDIAN VALUE

****

STATISTICAL PARAMETERS EXCLUDING NEGATIVE POINTS

****

2.99321 SMOOTH ICE DRAFT - MEAN VALUE

4.33340 SMOOTH ICE DRAFT - RMS VALUE

11.62277 SMOOTH ICE DRAFT - VARIANCE

3.39452 SMOOTH ICE DRAFT - STANDARD DEVIATION

[illegible] SMOOTH ICE DRAFT - MEDIAN VALUE

****

ANALYSIS OF ROUGH ICE, 50 KM SECTION

73374.2 NUMBER OF ROUGH ICE POINTS/[illegible]

72.68 PERCENTAGE ROUGH ICE

ROUGH ICE DISTRIBUTION - 50 KM SECTIONS

VALUES CLASSIFIED -1 TO 50 M BY 10 CM DIVISIONS
PROBABILITY DENSITY X 10**6/M, NORMALISED TO 100.00
PROBABILITY DENSITY TABLE - 10 CM BINS

METRES	.0+	.1+	.2+	.3+	.4+	.5+	.6+	.7+	.8+	.9+
-1 - 0	4.665881	28.211437	37.448661	7.[illegible]	[illegible]	[illegible]	[illegible]	[illegible]	[illegible]	[illegible]
0 - 1	29.[illegible]	37.[illegible]	[illegible]	[illegible]	[illegible]	[illegible]	[illegible]	[illegible]	[illegible]	[illegible]
1 - 2	1119.[illegible]	1237.[illegible]	[illegible]	[illegible]	[illegible]	[illegible]	[illegible]	[illegible]	[illegible]	[illegible]
2 - 3	1344.[illegible]	1199.[illegible]	[illegible]	[illegible]	[illegible]	[illegible]	[illegible]	[illegible]	[illegible]	[illegible]
3 - 4	1569.74029	1446.[illegible]	[illegible]	[illegible]	[illegible]	[illegible]	[illegible]	[illegible]	[illegible]	[illegible]
4 - 5	1579.11[illegible]	1541.[illegible]	[illegible]	[illegible]	[illegible]	[illegible]	[illegible]	[illegible]	[illegible]	[illegible]
5 - 6	941.[illegible]	946.[illegible]	[illegible]	[illegible]	[illegible]	[illegible]	[illegible]	[illegible]	[illegible]	[illegible]
6 - 7	726.[illegible]	656.[illegible]	[illegible]	[illegible]	[illegible]	[illegible]	[illegible]	[illegible]	[illegible]	[illegible]
7 - 8	421.[illegible]	468.[illegible]	[illegible]	[illegible]	[illegible]	[illegible]	[illegible]	[illegible]	[illegible]	[illegible]
8 - 9	352.[illegible]	421.[illegible]	[illegible]	[illegible]	[illegible]	[illegible]	[illegible]	[illegible]	[illegible]	[illegible]
9 - 10	[illegible]	370.[illegible]	[illegible]	[illegible]	[illegible]	[illegible]	[illegible]	[illegible]	[illegible]	[illegible]
10 - 11	257.71[illegible]	304.[illegible]	[illegible]	[illegible]	[illegible]	[illegible]	[illegible]	[illegible]	[illegible]	[illegible]
11 - 12	253.[illegible]	219.[illegible]	[illegible]	[illegible]	[illegible]	[illegible]	[illegible]	[illegible]	[illegible]	[illegible]
12 - 13	224.[illegible]	198.[illegible]	[illegible]	[illegible]	[illegible]	[illegible]	[illegible]	[illegible]	[illegible]	[illegible]
13 - 14	140.[illegible]	167.[illegible]	[illegible]	[illegible]	[illegible]	[illegible]	[illegible]	[illegible]	[illegible]	[illegible]
14 - 15	14.[illegible]	143.[illegible]	[illegible]	[illegible]	[illegible]	[illegible]	[illegible]	[illegible]	[illegible]	[illegible]
15 - 16	117.[illegible]	143.[illegible]	[illegible]	[illegible]	[illegible]	[illegible]	[illegible]	[illegible]	[illegible]	[illegible]
16 - 17	[illegible]	51.[illegible]	[illegible]	[illegible]	[illegible]	[illegible]	[illegible]	[illegible]	[illegible]	[illegible]
17 - 18	[illegible]	73.[illegible]	[illegible]	[illegible]	[illegible]	[illegible]	[illegible]	[illegible]	[illegible]	[illegible]
18 - 19	[illegible]	56.[illegible]	[illegible]	[illegible]	[illegible]	[illegible]	[illegible]	[illegible]	[illegible]	[illegible]
19 - 20	[illegible]	37.[illegible]	[illegible]	[illegible]	[illegible]	[illegible]	[illegible]	[illegible]	[illegible]	[illegible]
20 - 21	14.[illegible]	14.[illegible]	[illegible]	[illegible]	[illegible]	[illegible]	[illegible]	[illegible]	[illegible]	[illegible]
21 - 22	[illegible]	42.[illegible]	[illegible]	[illegible]	[illegible]	[illegible]	[illegible]	[illegible]	[illegible]	[illegible]
22 - 23	14.[illegible]	14.[illegible]	[illegible]	14.[illegible]	[illegible]	[illegible]	[illegible]	[illegible]	[illegible]	[illegible]
23 - 24	14.[illegible]	[illegible]	[illegible]	[illegible]	[illegible]	[illegible]	[illegible]	[illegible]	[illegible]	[illegible]
24 - 25	[illegible]	[illegible]	[illegible]	[illegible]	[illegible]	[illegible]	[illegible]	[illegible]	[illegible]	[illegible]
25 - 26	[illegible]	[illegible]	[illegible]	[illegible]	[illegible]	[illegible]	[illegible]	[illegible]	[illegible]	[illegible]
26 - 27	[illegible]	[illegible]	[illegible]	[illegible]	[illegible]	[illegible]	[illegible]	[illegible]	[illegible]	[illegible]
27 - 28	[illegible]	[illegible]	[illegible]	[illegible]	[illegible]	[illegible]	[illegible]	[illegible]	[illegible]	[illegible]
28 - 29	[illegible]	[illegible]	[illegible]	[illegible]	[illegible]	[illegible]	[illegible]	[illegible]	[illegible]	[illegible]
29 - 30	[illegible]	[illegible]	[illegible]	[illegible]	[illegible]	[illegible]	[illegible]	[illegible]	[illegible]	[illegible]
30 - 31	[illegible]	[illegible]	[illegible]	[illegible]	[illegible]	[illegible]	[illegible]	[illegible]	[illegible]	[illegible]
31 - 32	[illegible]	[illegible]	[illegible]	[illegible]	[illegible]	[illegible]	[illegible]	[illegible]	[illegible]	[illegible]
32 - 33	[illegible]	[illegible]	[illegible]	[illegible]	[illegible]	[illegible]	[illegible]	[illegible]	[illegible]	[illegible]
33 - 34	[illegible]	[illegible]	[illegible]	[illegible]	[illegible]	[illegible]	[illegible]	[illegible]	[illegible]	[illegible]
34 - 35	[illegible]	[illegible]	[illegible]	[illegible]	[illegible]	[illegible]	[illegible]	[illegible]	[illegible]	[illegible]
35 - 36	[illegible]	[illegible]	[illegible]	[illegible]	[illegible]	[illegible]	[illegible]	[illegible]	[illegible]	[illegible]
36 - 37	[illegible]	[illegible]	[illegible]	[illegible]	[illegible]	[illegible]	[illegible]	[illegible]	[illegible]	[illegible]
37 - 38	[illegible]	[illegible]	[illegible]	[illegible]	[illegible]	[illegible]	[illegible]	[illegible]	[illegible]	[illegible]
38 - 39	[illegible]	[illegible]	[illegible]	[illegible]	[illegible]	[illegible]	[illegible]	[illegible]	[illegible]	[illegible]
39 - 40	[illegible]	[illegible]	[illegible]	[illegible]	[illegible]	[illegible]	[illegible]	[illegible]	[illegible]	[illegible]
40 - 41	[illegible]	[illegible]	[illegible]	[illegible]	[illegible]	[illegible]	[illegible]	[illegible]	[illegible]	[illegible]
41 - 42	[illegible]	[illegible]	[illegible]	[illegible]	[illegible]	[illegible]	[illegible]	[illegible]	[illegible]	[illegible]
42 - 43	[illegible]	[illegible]	[illegible]	[illegible]	[illegible]	[illegible]	[illegible]	[illegible]	[illegible]	[illegible]
43 - 44	[illegible]	[illegible]	[illegible]	[illegible]	[illegible]	[illegible]	[illegible]	[illegible]	[illegible]	[illegible]
44 - 45	[illegible]	[illegible]	[illegible]	[illegible]	[illegible]	[illegible]	[illegible]	[illegible]	[illegible]	[illegible]
45 - 46	[illegible]	[illegible]	[illegible]	[illegible]	[illegible]	[illegible]	[illegible]	[illegible]	[illegible]	[illegible]
46 - 47	[illegible]	[illegible]	[illegible]	[illegible]	[illegible]	[illegible]	[illegible]	[illegible]	[illegible]	[illegible]
47 - 48	[illegible]	[illegible]	[illegible]	[illegible]	[illegible]	[illegible]	[illegible]	[illegible]	[illegible]	[illegible]
48 - 49	[illegible]	[illegible]	[illegible]	[illegible]	[illegible]	[illegible]	[illegible]	[illegible]	[illegible]	[illegible]
49 - 50	[illegible]	[illegible]	[illegible]	[illegible]	[illegible]	[illegible]	[illegible]	[illegible]	[illegible]	[illegible]

[illegible]

[illegible] FOR DISTRIBUTION = [illegible] OPTIONS
VALUES CLASSIFIED IN 0.5 & 1.0 M DIVISIONS

PROBABILITY DENSITY TABLE - [illegible] & 1 M BINS

METRES	0.0 - 0.5	0.5 - 1.0	0.0 - 1.0
-1 - 0	334.277[illegible]	1041.[illegible]	1364.[illegible]
0 - 1	2921.[illegible]	4991.[illegible]	7913.[illegible]
1 - 2	5019.[illegible]	[illegible]	11977.[illegible]
2 - 3	6139.[illegible]	7779.[illegible]	13918.[illegible]
3 - 4	7361.[illegible]	7[illegible]	14372.[illegible]
4 - 5	7[illegible]	[illegible]	11[illegible]
5 - 6	[illegible]	[illegible]	[illegible]
6 - 7	[illegible]	[illegible]	[illegible]
7 - 8	[illegible]	[illegible]	[illegible]
8 - 9	[illegible]	[illegible]	[illegible]
9 - 10	1977.[illegible]	1377.[illegible]	[illegible]
10 - 11	1166.[illegible]	1129.[illegible]	[illegible]
11 - 12	1059.[illegible]	1157.[illegible]	[illegible]
12 - 13	[illegible]	[illegible]	[illegible]
13 - 14	[illegible]	[illegible]	[illegible]
14 - 15	[illegible]	[illegible]	[illegible]
15 - 16	[illegible]	[illegible]	[illegible]
16 - 17	[illegible]	[illegible]	[illegible]
17 - 18	[illegible]	[illegible]	[illegible]
18 - 19	[illegible]	[illegible]	[illegible]
19 - 20	[illegible]	[illegible]	[illegible]
20 - 21	[illegible]	[illegible]	[illegible]
21 - 22	[illegible]	[illegible]	[illegible]
22 - 23	[illegible]	[illegible]	[illegible]
23 - 24	[illegible]	[illegible]	[illegible]
24 - 25	[illegible]	[illegible]	[illegible]
25 - 26	[illegible]	[illegible]	[illegible]
26 - 27	[illegible]	[illegible]	[illegible]
27 - 28	[illegible]	[illegible]	[illegible]
28 - 29	[illegible]	[illegible]	[illegible]
29 - 30	[illegible]	[illegible]	[illegible]
30 - 31	[illegible]	[illegible]	[illegible]
31 - 32	[illegible]	[illegible]	[illegible]
32 - 33	[illegible]	[illegible]	[illegible]
33 - 34	[illegible]	[illegible]	[illegible]
34 - 35	[illegible]	[illegible]	[illegible]
35 - 36	[illegible]	[illegible]	[illegible]
36 - 37	[illegible]	[illegible]	[illegible]
37 - 38	[illegible]	[illegible]	[illegible]
38 - 39	[illegible]	[illegible]	[illegible]
39 - 40	[illegible]	[illegible]	[illegible]
40 - 41	[illegible]	[illegible]	[illegible]
41 - 42	[illegible]	[illegible]	[illegible]
42 - 43	[illegible]	[illegible]	[illegible]
43 - 44	[illegible]	[illegible]	[illegible]
44 - 45	[illegible]	[illegible]	[illegible]
45 - 46	[illegible]	[illegible]	[illegible]
46 - 47	[illegible]	[illegible]	[illegible]
47 - 48	[illegible]	[illegible]	[illegible]
48 - 49	[illegible]	[illegible]	[illegible]
49 - 50	[illegible]	[illegible]	[illegible]

ROUGH ICE STATISTICAL PARAMETERS

2.700	ROUGH ICE DRAFT - MODAL VALUE
5.21426	ROUGH ICE DRAFT - MEAN VALUE
5.77191	ROUGH ICE DRAFT - RMS VALUE
17.57322	ROUGH ICE DRAFT - VARIANCE
4.29396	ROUGH ICE DRAFT - STANDARD DEVIATION
4.06502	ROUGH ICE DRAFT - MEDIAN VALUE

STATISTICAL PARAMETERS ZEROISING NEGATIVE POINTS

5.22737	ROUGH ICE DRAFT - MEAN VALUE
5.71092	ROUGH ICE DRAFT - RMS VALUE
17.51324	ROUGH ICE DRAFT - VARIANCE
4.19372	ROUGH ICE DRAFT - STANDARD DEVIATION
4.06502	ROUGH ICE DRAFT - MEDIAN VALUE

LEVEL/SOUTH ICE LENGTH/DRAFT ANALYSIS
(LENGTHS & DRAFTS = SUCCESSIVE SEGMENTS)

LEVEL ICE LENGTH (M)	LEVEL ICE MEAN DRAFT (M)	RIDGE ICE LENGTH (M)	RIDGE ICE MEAN DRAFT (M)
12.	2.	114.	3.11717
10.	3.72409	432.	3.74733
91.	3.42273	136.	3.21533
1.	3.47965	21.	1.11332
74.	3.45204	1.	3.36192
1.	3.47777	1.	3.45573
3.	3.42517	11.	3.56374
17.	3.43327	15.	3.56371
10.	3.46975	61.	3.79330
14.	3.39759	39.	1.11174
5.	3.41113	1.	3.47774
12.	3.47737	14.	3.19243
11.	3.39933	5.	3.77529
13.	3.39253	1.	3.96343
14.	3.31161	2.	3.39827
19.	3.38383	2.	3.37761
13.	3.39273	2.	3.13911
1.	3.26169	337.	3.14552
14.	3.33330	2.	3.34755
21.	3.42231	23.	3.51127
19.	3.43355	53.	3.56155
14.	3.25752	0.	0.
2.	3.47221	3.	3.44777
1.	3.47776	3.	3.44777
11.	3.38845	345.	3.60374
19.	3.39493	113.	3.51147
13.	3.36756	38.	3.44539
15.	3.3744	12.	3.44
10.	3.33359	4.	3.36
2.	3.39263	2.	3.44
11.	3.41555	4.	3.23
2.	3.37	19.	3.37
13.	3.37386	3.	3.25
27.	3.35213	166.	3.33
155.	3.26425	10.	3.31
11.	3.33	1.	3.77
15.	1.38019	9.	1.15
34.	1.34221	2.	3.27
37.	3.31321	29.	3.27
41.	1.32357	31.	3.25
155.	3.31190	10.	1.05
12.	3.72233	45.	3.53
31.	3.46955	1.	3.52
17.	3.76366	2.	3.09
13.	3.72296	18.	3.47
15.	2.57335	4.	3.15
14.	3.17543	3.	3.04
33.	2.34431	2.	3.07

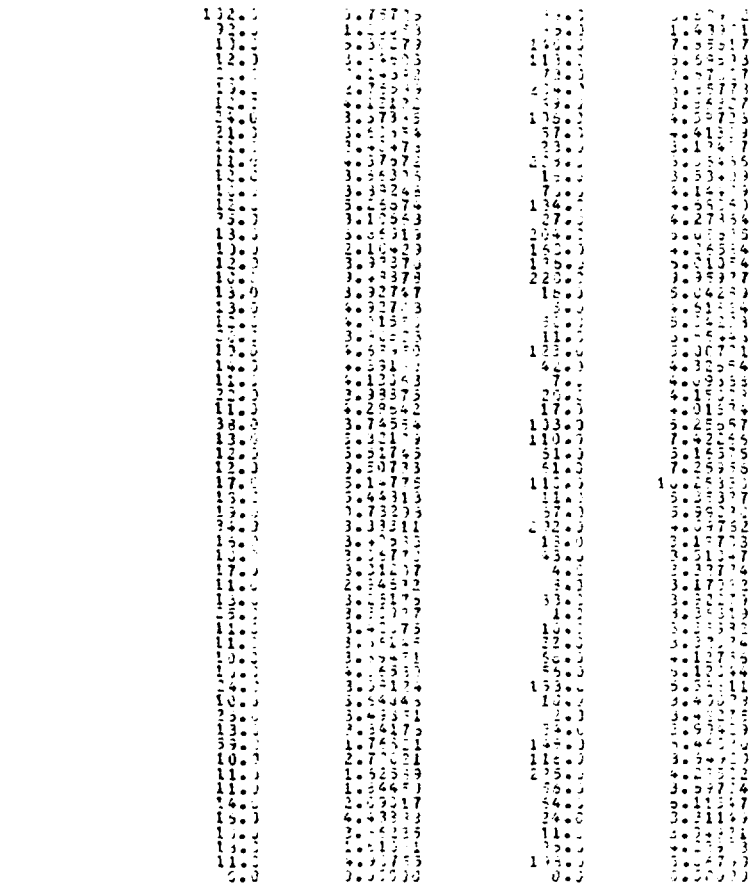

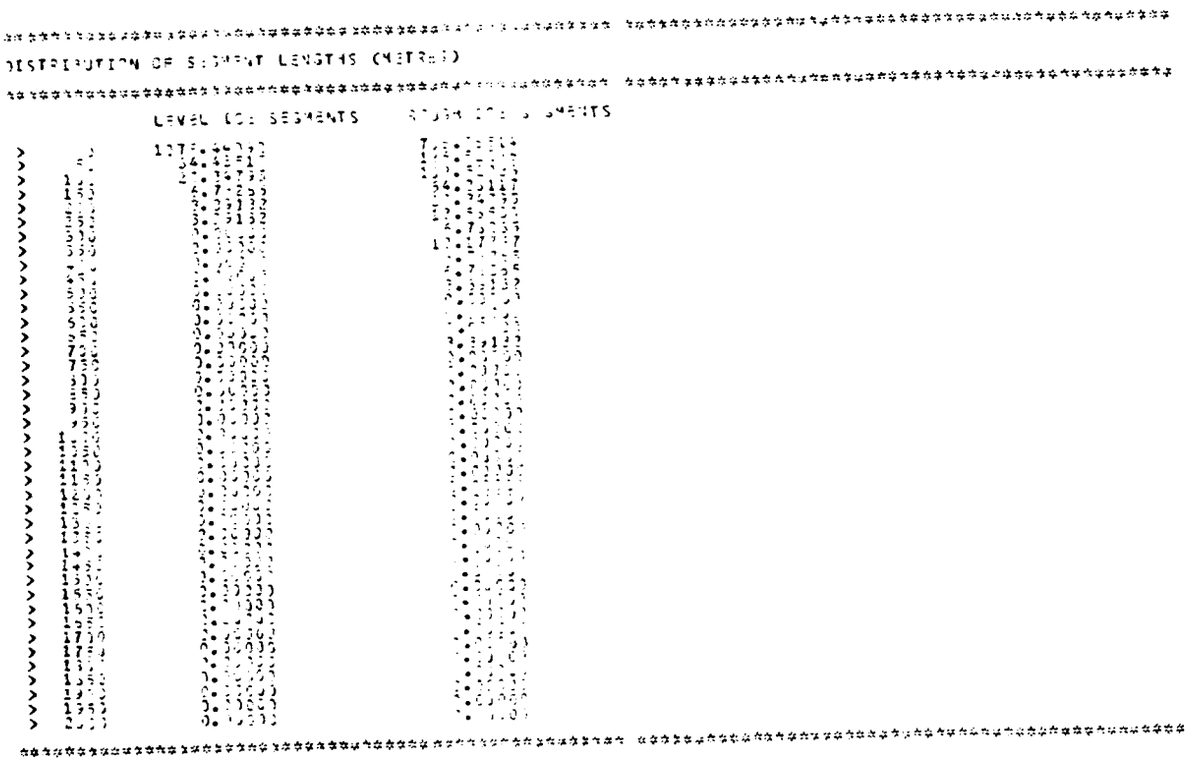

DISTRIBUTION OF MEAN DRAFTS (METRIC)

	LEVEL ICE		RIDGE ICE	
	NO. OF SEGS	TOT. LENGTH	NO. OF SEGS	TOT. LENGTH
> -1.0				
> -0.5				
> 0.0				
> 0.5				
> 1.0				
> 1.5				
> 2.0				
> 2.5				
> 3.0				
> 3.5				
> 4.0				
> 4.5				
> 5.0				
> 5.5				
> 6.0				
> 6.5				
> 7.0				
> 7.5				
> 8.0				
> 8.5				
> 9.0				
> 9.5				
> 10.0				
> 10.5				
> 11.0				
> 11.5				
> 12.0				
> 12.5				
> 13.0				
> 13.5				
> 14.0				
> 14.5				
> 15.0				
> 15.5				
> 16.0				
> 16.5				
> 17.0				
> 17.5				
> 18.0				
> 18.5				
> 19.0				
> 19.5				
> 20.0				
> 20.5				
> 21.0				
> 21.5				
> 22.0				
> 22.5				
> 23.0				
> 23.5				
> 24.0				
> 24.5				
> 25.0				
> 25.5				
> 26.0				
> 26.5				
> 27.0				
> 27.5				
> 28.0				
> 28.5				
> 29.0				
> 29.5				
> 30.0				

ANALYSIS OF PRESSURE RIDGES - DRAFT & SPACING
(RAYLEIGH CRITERION RELATIVE TO A 2.5M DRAFT)

LISTING OF RIDGE DRAFT & SPACING/5[illegible] KM SECTION

RIDGE DRAFT (M)	RIDGE SPACING (M)				
6.1[illegible]	15.0				
3.7[illegible]3	35.0				
5.44[illegible]3	[illegible]				
3.37[illegible]7[illegible]	131.0				
3.9[illegible]	67.0				
12.23116	27.0	5.60114	65.0	4.44470	13.0
6.42276	57.0	5.01420	100.0	[illegible]	17.0
3.15795	45.0	4.22153	44.0	4.62071	42.0
3.05470	41.0	2.67496	21.0	3.92059	14.0
4.65372	47.0	5.19592	12.0	4.21719	5[illegible]
7.17930	65.0	5.35552	46.0	5.06139	27.0
3.74566	65.0	5.21[illegible]	44.0	2.54282	12.0
7.74796	64.0	5.44546	15.0	3.71044	24.0
3.77469	30.0	4.50265	44.0	5.65[illegible]	22.0
5.47724	7.0	2.67214	111.0	2.69[illegible]4	[illegible]
5.1[illegible]	23.0	4.59790	38.0	5.3[illegible]66	74.0
[illegible].74[illegible]	120.0	4.14[illegible]	17.0	[illegible].7[illegible]	22.0
[illegible].5[illegible]73	[illegible]	2.21[illegible]	[illegible]	[illegible].4[illegible]	17.0
[illegible]73	[illegible]	4.[illegible]214	130.0	2.[illegible]	15.0
7.56544	43.0	6.51594	45.0	2.7442[illegible]	21.0
4.41212	23.0	2.50724	45.0	2.[illegible]	15.0
3.20[illegible]	53.0	5.66[illegible]	155.0	2.5[illegible]	11.0
2.77555	25.0	12.617[illegible]	147.0	[illegible].65[illegible]2	67.0
3.20[illegible]94	67.0	1[illegible].99[illegible]1	17.0	9.[illegible]7	55.0
3.5[illegible]454	52.0	1[illegible]	[illegible]	9.[illegible]5	45.0
3.47020	[illegible]	11.6[illegible]57	[illegible]	6.52[illegible]9	45.0
[illegible]	39.0	5.37922	[illegible]	13.76[illegible]0	55.0
4.61[illegible]	[illegible]	5.21514	[illegible]	1[illegible].7[illegible]	[illegible]
3.21[illegible]	17.0	5.40[illegible]	11[illegible]	4.57[illegible]	[illegible]
[illegible]	15.0	5.32152	41.0	7.24321	95.0
5.54052	23.0	4.05[illegible]	43.0	17.66[illegible]	[illegible]
6.16147	57.0	2.09[illegible]	[illegible]	11.16[illegible]0	777.0
2.66754	54.0	2.54[illegible]	[illegible]	21.[illegible]70	63.0
13.55710	20.0	5.77504	[illegible]	23.76[illegible]	[illegible]

DISTRIBUTION OF PRESSURE RIDGE DRAFTS (-1.0 - 50.0)

DRAFT (M)	NO. IN SECTION	NO. PER 100 KM	NO. PER KM
> -1.	6	0.0	0.0
> 0.	0	0.0	0.0
> 1.0	0	0.0	0.0
> 2.0	81	30.9	0.3
> 3.0	110	42.0	0.4
> 4.0	73	27.9	0.3
> 5.0	67	25.6	0.3
> 6.0	46	17.6	0.2
> 7.0	20	7.6	0.1
> 8.0	17	6.5	0.1
> 9.0	15	5.7	0.1

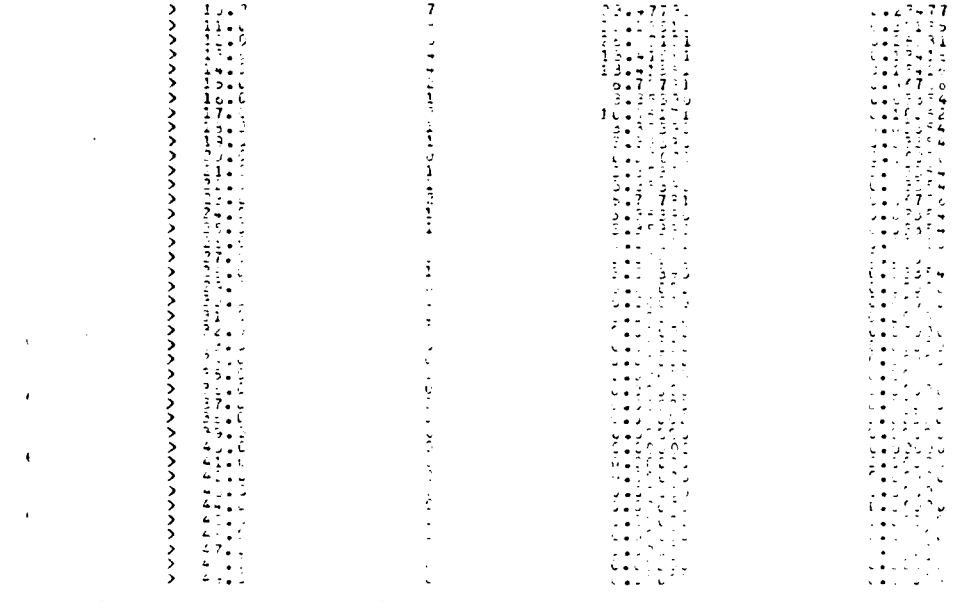

STATISTICAL PARAMETERS - TOTAL PRESSURE PROBES

PRESSURE PROBES - TOTAL NUMBER

PRESSURE PROBES - NUMERATOR

PRESSURE PROBES - MEAN DRAFT

PRESSURE PROBES - RMS DRAFT

PRESSURE PROBES - VARIANCE

PRESSURE PROBES - STANDARD DEVIATION

PRESSURE PROBES - MEDIAN DRAFT

STATISTICAL PARAMETERS - PRESSURE RIDGES > [illegible] M

194.1	PRESSURE RIDGES - TOTAL NUMBER
4.5[illegible]97	PRESSURE RIDGES - NUMBER/KM
3.74[illegible]37	PRESSURE RIDGES - MEAN DRAFT
9.73[illegible]70	PRESSURE RIDGES - RMS DRAFT
16.5[illegible]763	PRESSURE RIDGES - VARIANCE
4.[illegible]18	PRESSURE RIDGES - STANDARD DEVIATION
7.2[illegible]7	PRESSURE RIDGES - MEDIAN DRAFT

STATISTICAL PARAMETERS - PRESSURE RIDGES > 9.[illegible] M

42.1	PRESSURE RIDGES - TOTAL NUMBER
2.07[illegible]42	PRESSURE RIDGES - NUMBER/KM
13.81[illegible]46	PRESSURE RIDGES - MEAN DRAFT
14.29[illegible]61	PRESSURE RIDGES - RMS DRAFT
20.[illegible]4[illegible]8	PRESSURE RIDGES - VARIANCE
4.[illegible]967	PRESSURE RIDGES - STANDARD DEVIATION
12.01[illegible]02	PRESSURE RIDGES - MEDIAN DRAFT

25.44[illegible]44 PRESSURE RIDGE - MAXIMUM DRAFT

DISTRIBUTION OF PRESSURE RIDGE SPACING
(0 TO [illegible] M BY 20 M INTERVAL)

SPACING	NUMBER IN BIN	PROBABILITY	CUM. PRO
> [illegible]	42[illegible].22277	[illegible].[illegible]10	[illegible].[illegible]91
> [illegible]	4[illegible].24[illegible]	[illegible].[illegible]19	[illegible].[illegible]10
> 4[illegible]	3[illegible].[illegible]3[illegible]	[illegible].[illegible]13	[illegible].[illegible]31
> [illegible]	11[illegible].[illegible]2[illegible]	[illegible].[illegible]5	[illegible].[illegible]96
> [illegible]	[illegible].[illegible]3[illegible]	[illegible].[illegible]5	[illegible].[illegible]1
> 1[illegible]	67.[illegible]1[illegible]6	[illegible].[illegible]3[illegible]	[illegible].[illegible]72
> 14[illegible]	43.[illegible]0[illegible]74	[illegible].[illegible]2[illegible]	[illegible].[illegible]25[illegible]
> 14[illegible]	10.[illegible]4[illegible]1	[illegible].[illegible]1	[illegible].[illegible]7[illegible]

>	10	20.12341	0.61035	0.94661
>	11	5.71791	0.70472	0.97215
>	21	3.58397	0.80214	0.95503
>	12	10.41366	0.87317	0.98321
>	24	5.71791	0.91431	0.98778
>	13	2.46106	0.94727	0.99736
>	33	5.71791	0.97421	0.97214
>	22	5.71791	0.98904	0.97645
>	34	3.58397	0.99214	0.99573
>	35	3.58397	0.99214	0.99573
>	23	0.00001	0.00000	0.33073
>	44	30.19513	0.91437	1.00000

****

REGRESSION CORRELATION COEFFICIENTS
PRESSURE RIDGE SPACING DISTRIBUTION

****

CORRELATION COEFFICIENT 0.91437 LOG NORMAL DISTRIBUTION

CORRELATION COEFFICIENT 0.99548 EXPONENTIAL DISTRIBUTION

CORRELATION COEFFICIENT 0.99044 LOGARITHMIC DISTRIBUTION

CORRELATION COEFFICIENT 0.91439 LOG E NORMAL DISTRIBUTION

****

APPENDIX 4

Papers enclosed

PROCESSES DETERMINING THE BOTTOM TOPOGRAPHY OF MULTIYEAR ARCTIC SEA ICE

Peter Wadhams
Scott Polar Research Institute,
University of Cambridge, England.

Seelye Martin
Department of Oceanography,
University of Washington, Seattle, Wa.

INTRODUCTION

In May 1987 the first systematic imaging was carried out of the bottom surface of the Arctic ice cover, using sidescan sonar from a submarine (Wadhams, 1988). The results showed that undeformed first-year ice has a smooth bottom topography broken up by occasional long cracks, whereas undeformed multi-year ice is covered with dome-like features (e.g. fig. 1). These have horizontal scales of 10-50 m and vertical scales of 0.5 - 1 m. They are scattered apparently at random over the surface of the ice, and there appear to be no corresponding hollows; thus the topography resembles an inverted version of the lunar surface, with domes instead of craters.

In this paper we address the question of the formation mechanism for these under-ice structures. A number of possible mechanisms suggest themselves.

The nature of multi-year ice is one of the many scientific problems that have been addressed by W F Weeks, and in a paper by Cox and Weeks (1974) we find the only known temperature-salinity section across a hummock-depression-hummock sequence in a multi-year floe. The authors found a wavelength of 12 m between successive hummocks or domes, with a relief of about 1 m in a floe of mean thickness 3 m. These contours are useful as a clue to the processes which have occurred within the floe.

ORIGIN OF THE TOPOGRAPHIC FEATURES

Possible explanations for these features fall into two groups.

1. They are related to the summer melt cycle which multi-year ice has undergone. In support of this idea is the observation that the scale of the domes, and the more or less random distribution of them over the floe surface, resemble the distribution of upper surface melt ponds during the Arctic summer. Fig. 2 shows a typical aerial photograph of such ponds.
2. They represent the almost-vanished relics of worn-down pressure ridges created years earlier in the life of the floe. Against this idea is the observation that there is no linearity to the distribution of the domes, and also the fact that in over 1000 km of sidescan record (representing 10^3 km^2 of ice surface) there is no intermediate case of a ridge worn down to almost the point where it looks like a sequence of domes. In every area of multi-year ice there is a clear distinction between the undeformed ice surface, with its gently sloping topography of bulges, and ridges which show clear linearity and strong angularity to the ice blocks.

We therefore tentatively reject the second explanation, and explore mechanisms related to the melt-freeze cycle.

THE MELT-FREEZE CYCLE

When a first-year ice sheet experiences its first summer melt period, some 30 cm of ablation occurs from the upper surface in the form of snow and ice melt (Untersteiner, 1967). This meltwater gathers in melt ponds and pools on the upper surface of the floe, then drains to the underlying ocean. Possible pathways for drainage are:-

a) through holes melted in the bottom of the pools,
b) by channels cut to nearby cracks and leads,

c) by slow percolation through the ice sheet via grain boundaries,
d) through wide brine drainage channels which have opened up as far as the ice surface.

The extent, or even the existence, of mechanism (c) is unknown, although it can be assumed that surface meltwater plays a role in the mechanism of flushing by which extensive desalination of first-year ice occurs in summer. Note that because the water is fresh it cannot flow into the underlying ocean through narrow brine drainage channels, in that because the ice temperature generally lies below 0°C, the water would freeze solid and block these small channels. Wider brine drainage channels do, however, provide a pathway. It has been observed in connection with research on the behaviour of oil deposited under first-year ice that the larger brine drainage channels open up and melt their way upward to the upper ice surface in spring, possibly because the sides of the channel act as a waveguide, concentrating solar radiation within the channel. In the case of oil, they provide an upward pathway, and in the case of meltwater a possible downward pathway; alternatively the channel may simply provide a start point for the growth of a larger thaw hole to permit macroscopic drainage.

When a surface melt pool first forms, it is very shallow and positions itself in a random minor depression in the almost perfectly flat surface of the first-year floe. Once a pool of any thickness, however small, has been created, however, its low albedo causes preferential absorption of solar radiation and consequent warming of the water in the pool. It will thus melt its way down into the floe by eroding its own bottom. The difference in elevation between the bottoms of melt pools and bare ice therefore increases as summer progresses (but before drainage empties the pools) until it is several cm or even tens of cm. Some observations from Fiennes (1984) of the depth of a single melt pool over a period of 23 days may be apposite here: he found a depth increasing from 35 cm on July 10 to a maximum of 44 cm in mid-July, falling to 13 cm by August 1 as drainage proceeded.

The presence of a warm water pool at the top of the ice sheet should also cause the bottom of the sheet to melt more rapidly beneath the melt pool. A series of under-ice depressions should therefore be created, with lateral dimensions similar to those of the overlying surface melt pools. The existence of such under-ice cavities has been noted in the work of Hanson (1965) and others, although there is scarcely any experimental data on sizes, aspect ratios or distributions of the observed cavities. During the summer we therefore expect a first-year floe to begin to develop an underside topography of depressions, reflecting the surface melt pool topography.

How does a topography of depressions translate into the topography of bulges seen in winter multi-year floes? We believe that the answer lies in the fate of the meltwater that has passed into the ocean via one of the mechanisms (a) to (d) listed above, and which then gathers in the depressions to form under-ice melt pools.

FORMATION AND FATE OF UNDER-ICE MELT POOLS

Fresh water which has run off from the ice surface, or which is generated by melting of the ice underside, will collect prefentially under portions of the ice bottom surface with lower draft. Thus sub-ice depressions tend to form into what Hanson (1965) defined as "under ice melt ponds". The effect has been described extensively (e.g. Nansen, 1897; Zubov, 1945; Untersteiner and Badgley, 1958), and the subsequent evolution of the ponds has been studied and investigated in laboratory experiments by Martin and Kauffman (1974). Briefly, what happens is as follows (see fig. 3).

The trapped fresh or brackish water is at its freezing point, i.e. at or near 0°C, while the underlying polar surface water is at its own freezing point of -1.6°C or lower. Therefore freezing of the fresh water takes place at the interface (even in summer), creating a thin skim of ice on the inverted surface of the melt pond (fig. 3). Observations show that the sheet thus formed reaches a thickness of 2-10 cm. The space between the sheet and the lower surface of the floe becomes filled with a mass of loosely packed ice crystals, with a preponderance of thin vertical crystals running from the bottom of the ice floe to the top of the new ice sheet. This effect was explained by Martin and Kauffman (1974) in terms of a density inversion created in the fresh water layer by the rapid diffusion of heat relative to salt, causing high Rayleigh number convection whereby supercooled water rises to the floe bottom to nucleate into thin vertical interlocking ice crystals.

As summer proceeds, the horizontal ice sheet forming the bottom of the melt pond grows thicker and migrates slowly upwards. This occurs because freezing at the top of the sheet releases heat which flows through the ice to the lower surface, where it warms the lower interface to slightly above the freezing curve, causing melting. This upward migration of the

ice sheet at the bottom of the pond means that the pond is shrinking upwards into its own depression and ends up not quite filling that depression.

Martin and Kauffman showed that the processes occurring in under-ice melt ponds represent an efficient, and perhaps the only important, way of growing new ice in summer within the Arctic.

When summer ends, the air temperature lowers and freezing begins. We have little experimental or observational knowledge of what happens at this point. If the melt pond has already filled completely with ice from internal processes (the horizontal interface sheet growing thicker and/or the vertical crystal mesh filling the remainder of the pond, then clearly the bottom of the pond's ice sheet simply provides a start point for the new season's growth of congelation ice. Beacuse the pond lies under a depression in the top surface (from which the water by now has probably drained), the ice is locally thinner and so the growth rate will be somewhat greater than that of the thicker ice around the pond. Nevertheless, we surnmise that the differential growth rate is low enough, and the initial differential ice draft great enough, that the difference is never made up.

Thus we have one plausible mechanism for the observed bulges. The matrix of flat ice surrounding the bulges actually comprises the lower surfaces of refrozen under-ice melt ponds, which have rectified the depressions in the ice created during the summer melt, but which still lie at a lower draft than the regions of the floe which never harboured ponds on the upper or lower surface. These regions stand proud to form the gentle bulges observed (fig. 4). We believe that this is the most likely explanation.

Another possibility, however, is the complete opposite. If the under-ice melt ponds still contain fresh water at the end of summer, this will freeze and thus expand. If the process occurs slowly enough, the flat ice cover on the under-ice pond could bulge out below due to the change in volume. Since this process would be taking place with the ice sheet surrounded by water at its freezing point, the ice may be ductile enough to bulge outward without cracking. It is then the ponds themselves which form the bilges. This process could be verified by laboratory experiments. It seems unlikely, however, that reliefs of the order of 1 m could be produced in this way.

TESTS AND IMPLICATIONS

How do we test this model? An indirect test, which would indicate whether melt ponds are indeed connected with the mechanism of dome generation, would be to measure the spatial frequency of domes and the distribution of dome diameters from all the available sidescan sonar imagery, and compare the results with distributions of melt pond frequencies and pond diameters (and the distribution of dimensions of the regions left between melt ponds) obtained from aerial photography of first-year floes in summer. This study is in progress.

A direct test would be to carry out careful coring studies across second-year ice floes at different stages of the winter. A pattern should emerge whereby the zones of lower draft possess lenses of low salinity ice near the bottom of the ice sheet, whereas the zones of greater draft do not. Further direct tests could be done in summer and autumn, examining the evolution and subsequent freeze-up of a few under-ice melt ponds on a first-year floe. Finally, many aspects of the process can be reproduced in laboratory experiments .

If the model proves to be valid, the main implication would be that the formation of under-ice melt ponds in first-year floes in summer must be a universal process, rather than a curiosity. This would have important consequences for the thermodynamic modelling of Arctic sea ice, since it implies that significant ice growth must occur under existing ice sheets in summer, so that summer ablation is replaced rather rapidly by accretion at the lower surface.

Finally, whatever mechanism proves to be the explanation for under-ice domes, the existence of this kind of topography under multi-year ice has various implications of its own. Models of acoustic propagation under sea ice usually assume that scattering by pressure ridges is the chief source of transmission loss (e.g. Burke and Twersky, 1966; Guoliang and Wadhams, 1989), while it is now necessary to include the under-ice bulges as scattering elements. Similarly, models which attempt to infer ice-water drag coefficients from parameters of under-ice roughness must take account of roughness elements possessed by undeformed multi-year floes. Finally, the clear characterisation of multi-year ice made possible by its underside topography enables sidescan sonar imagery when recorded concurrently with other remote sensing imagery to be used as a validation technique for passive or active microwave, since unequivocal identification of ice type is now possible.

ACKNOWLEDGEMENTS

PW acknowledges the support of the Office of Naval Research under contract N00014-82-C-0064 to Science Applications International Corporation, Polar Oceans Division..

REFERENCES

Burke, J.F. and V. Twersky (1966). Scattering and reflection by elliptically striated surfaces. *J. Acoust. Soc. Am., 40*, 883-895.

Cox G.F.N. and W.F. Weeks (1974). Salinity variations in sea ice. *J. Glaciol., 13*(67), 109-120.

Fiennes, R. (1984). Notes on ice melt. From *Report on Scientific Work of the Transglobe Expedition 1979-1982*, p.302.

Guoliang, J. and P. Wadhams (1989). Travel time changes in a tomography array caused by a sea ice cover. *Progress in Oceanogr.*, in press.

Hanson, A.N. (1965). Studies of the mass budget of Arctic pack-ice floes. *J. Glaciol., 5*, 701-709.

Martin, S. and P. Kauffman (1974). The evolution of under-ice melt ponds, or double diffusion at the freezing point. *J. Fluid Mech., 64*, 507-527.

Nansen, F. (1897). *Farthest North, 1*, 457-459. Harper, New York.

Untersteiner, N. (1967). Natural desalination and equilibrium salinity profile of old sea ice. In *Physics of Snow and Ice* (ed. H. Oura), *1*, 569-577. Inst. of Low Temperature Science, Sapporo.

Untersteiner, N. and F.I. Badgley (1958). Preliminary results of thermal budget studies on Arctic pack ice during summer and autumn. In *Arctic Sea Ice, 85-92*. Nat. Acad. Sci. / Nat. Res. Counc. publn. 598, Washington.

Wadhams, P. (1988). The underside of Arctic sea ice imaged by sidescan sonar. *Nature, Lond., 333*, 161-164.

Zubov, N. (1945). *Arctic Ice* (Eng. trans.) US Navy Electronics Lab., San Diego.

FIGURES

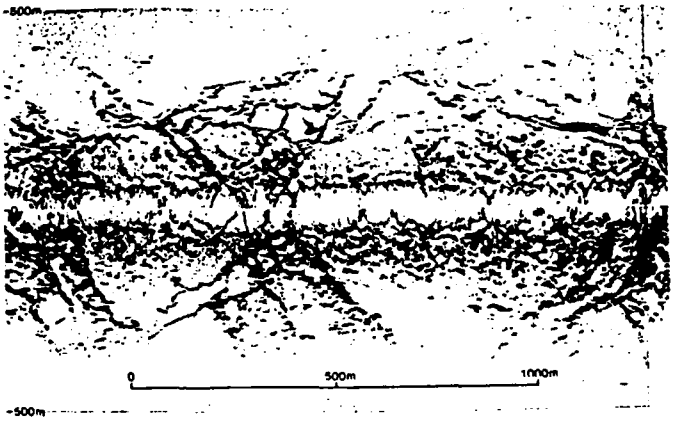

Fig. 1 A section of sidescan sonar profile from the Arctic Ocean showing two multi-year floes. Transducer depth 75 m.

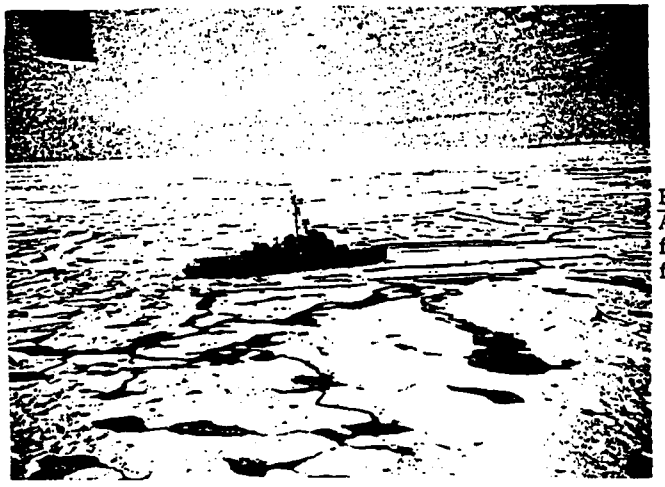

FIG.2 . Surface melt pools in August in multi-year ice (near field) and first-year ice (far field).

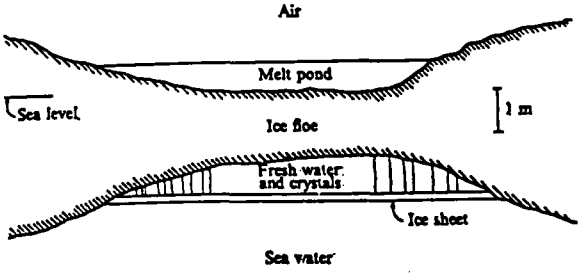

FIG.3 . Schematic diagram of an under-ice melt pool.

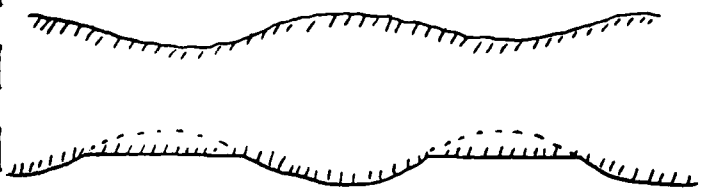

FIG.4 . Schematic diagram of under-ice topography after refreezing of under-ice melt pools.

7/27/89 Submitted to EOS

CONCURRENT REMOTE SENSING OF ARCTIC SEA ICE FROM SUBMARINE AND AIRCRAFT

P. Wadhams[1], J.C. Comiso[2], A.M. Cowan[3], J. Crawford[4], G. Jackson[5],
W. Krabill[6], R. Kutz[2], C.B. Sear[3], R. Swift[7] and W.B. Tucker[8].

In May 1987, the first concurrent remote sensing of Arctic sea ice from the top and the underside was performed. A submarine, equipped with sidescan and upward looking sonar, collaborated with two remote sensing aircraft equipped with passive microwave, synthetic aperture radar (SAR), infrared sensor, and laser profilometer. By careful registration of the three tracks it has been possible to find relationships between ice type, ice morphology, SAR backscatter and microwave brightness temperatures. The key to the process has been the sidescan sonar's ability to identify ice type through differences in characteristic topography.

INTRODUCTION

A collaborative remote sensing experiment involving a submarine and two aircraft travelling along identical tracks took place in the Arctic Ocean in May 1987. This was a unique experiment in that it was the first time that under-ice imagery as well as ice draft profiles could be compared directly with the output of ice surface remote sensing systems, including passive microwave, synthetic aperture radar (SAR), and laser profilometer. The results provide the first extensive validation of SAR and passive microwave performance in terms of definitely known ice types and ice thicknesses. The value of this

experiment lies with the varied sensor types which have been co-registered to the SAR image, such that inferences can be drawn by contrasting the signatures of the various sensors.

The submarine was equipped with an EDO Western model 602 sidescan sonar towfish, mounted on her upper casing and feeding an EDO 706 sidescan mapping system operating at 100 kHz. The submarine was also equipped with a narrow-beam 48 kHz upward-looking sonar with paper chart and digital outputs. A NASA P-3A aircraft was equipped with a set of passive microwave sensors, Airborne Oceanographic Lidar (AOL), a PRT-5 infra-red radiometer, and aerial cameras. The other aircraft was a Cessna Conquest of Intera Technologies Ltd., Calgary, Alberta, equipped with the STAR-2 X-band HH-polarization SAR giving wide swath (65 km) imagery. The Cessna flew at 10,000 m throughout; the P-3A was flown partly at high altitude (6000 m) for good spatial coverage and partly at low altitude (245 m) for good resolution and to allow use of the AOL.

The submarine undertook four 24-hour legs of ice profiling, proceeding from the North Pole towards the coast of Greenland, then eastward to the entrance of Fram Strait and southward through the Greenland Sea. Each leg was overflown close to its time of completion by the two aircraft, operating from bases in northern Canada (Alert), Greenland (Thule) and Svalbard. In this paper we report results of the analysis of a portion of the joint dataset, obtained in the heavily ridged region north of Greenland at about 85^{0}N on May 20th. Analysis of the complete dataset will be reported in future papers.

POSITIONING

Positioning is a critical part of the data reduction and analysis procedure, since the concurrent data were captured from three separate

platforms along a pre-arranged sampling track. The submarine, Intera aircraft and P-3A aircraft were all navigated with inertial navigation systems (INS). In addition, for the P3-A, positioning information from a Motorola Eagle Global Positioning System (GPS) receiver was recorded along with the INS data. During the May 20th mission, a four satellite GPS constellation was visible for a period of approximately 2.5 hours, during which the high altitude microwave observations were captured. Aerial photographs were also obtained with a T-11 23 cm format camera as well as with a 35 mm Flight Research camera, both of which place the time of day on an inset associated with each photograph.

Our approach to post-flight positioning was to use the GPS information and the high altitude aerial photography to register the data from the P-3A aircraft sensors to the SAR image. In the sample track length of 191 km, which is analyzed in this study, a total of 20 features (largely leads) were unambiguously recognized in both the SAR imagery and the aerial photography. We were able to reconcile points between east- and west-bound passes in the same region to within less than 300 m. During the low altitude portion of the mission, the positioning of the data was determined by using the INS information corrected with the last available GPS-determined position. We were able to correct the INS registered data through comparison of the low altitude (245 m) aerial photographs with the previously registered SAR image using 12 unambiguous features. In our estimation, the laser profiling data are registered to the SAR imagery to within $\pm$ 85 m (five SAR pixels).

The sonar records from the submarine were co-registered with the SAR imagery by matching features in the sidescan sonar image with those of the SAR. It was easy to recognize floes, ridges and leads on each set of imagery and many coincident points could be found, giving an estimated cross-track accuracy

of registration of better than five SAR pixels. The submarine track was overlaid on the SAR imagery and in this way could be compared with the P-3A track and associated data sets.

SENSOR COMPARISONS

3.1 Active and Passive Microwave Imagery

The microwave sensors are ideal for monitoring sea ice cover because of their ability to penetrate cloud and darkness. The passive microwave system consists of an Electrically Scanning Microwave Radiometer (ESMR) which operates at 19 GHz, and a set of multichannel sensors called Advanced Multichannel Microwave Radiometer (AMMR) consisting of 37 GHz and 18 GHz dual polarized radiometers and a 21 GHz channel operating at vertical polarization only. ESMR has a beam width of 3^{0} and covers a spatial area from -45^{0} to 55^{0} with 39 beam positions. The AMMR channels have beam widths of about 6^{0} and were set at 50^{0} so as to be compatible with the Scanning Multichannel Microwave Radiometer (SMMR) on board the Nimbus-7 satellite. The X-band SAR system on board the Intera aircraft has a resolution of 16 m and a swath width of 64 km. The image is presented in the form of pixels, each of which represents relative radar backscatter.

An example of coverage over sea ice by both active and passive sensors is shown in Figure 1. The P-3A aircraft was first flown from west to east at an altitude of 6,000 m. A second pass was then flown from east to west, offset so that the AMMR viewed the same area of interest at the same altitude. Finally a low altitude track at 220 m was flown over the previous AMMR track. Figure 1a shows color coded ESMR imagery collected during the high-altitude eastbound leg, Figure 1b shows the SAR image over the same general area, while

Figure 1c shows ESMR imagery collected during the westbound leg. The location of the AMMR footprint in the westbound pass is shown by the color-coded stripe in Figure 1b. Some ice features common to both sensors, especially leads and areas of first-and multi-year ice have been indicated with identifying arrows.

In the ESMR imagery, first-year ice cover has the highest brightness temperature (designated by pink) because the ice is saline, resulting in high effective emissivity. Areas of multi-year ice show much more variability with low values (light brown and orange) where the ice is relatively flat and has snow cover and slightly higher brightness temperature values (dark brown) in heavily ridged areas. Areas of open water exhibit the lowest brightness temperature (green and blue). By contrast, the SAR imagery shows low backscatter values for open water inside the ice pack, slightly higher values for thin and first-year ice, higher values for multiyear ice and the highest values for ridged ice (Lyden et al., 1984). Because they are sensitive to different physical properties of the ice, the active and passive sensors could thus complement each other and can be used to improve discrimination of different ice types. For example, whenever undeformed young or new ice is difficult to differentiate from calm open water in the SAR image because of almost identical backscatter, the passive microwave data can be used to remove the ambiguity because of the large contrast in the emissivity of these two surfaces. Also, when the snow/ice interface of a multiyear ice floe is saline, as can happen through various mechanisms (Tucker et al., 1987), the brightness temperature of this ice type would be very similar to that of first-year ice. In this case, the SAR data can be used to better establish the ice type because of the large difference in backscatter between multiyear ice and undeformed first year ice. The interpretation of first-year, multi-year ice and leads was

aided by notes taken by an ice observer during the flight and by video and still photography.

3.2. Comparison with sonar, infrared, and laser.

Figure 2 is a composite scene developed using co-registered upward and sidescan sonar data, X-band SAR imagery, passive microwave radiometry, and laser profiling information. The SAR (Fig. 2d) scene which is approximately 7 km by 2 km, has had a submarine ground track superimposed on it. This section was selected for presentation because it contains examples of open leads, recently refrozen leads, first-year ice, and deformed multi-year ice with well defined ridging. The upward sonar profile is shown in Figure 2b, and the analog side-scan sonar scene in Figure 2c. A profile of the SAR backscatter values extracted from the submarine track is shown in Figure 2a. Corresponding surface ice topography obtained with the AOL laser profilometer is provided in Figure 2e, along with an infra-red ice surface temperature profile from the PRT-5 (Figure 2f), and a cross-section of the 18 and 37 GHz ice emissivities acquired with the AMMR (Figure 2g). It can be seen that there are strong relationships among the signatures of the various sensors to the quite varied ice types. The center of the SAR image is dominated by a section of open lead (white arrow), a the large area of first year ice (dark green), and an expanse of highly deformed multi-year ice (yellow), especially to the west (left) of the lead, with the lightest yellow (highest backscatter) corresponding to ridges. The sidescan sonar shows mainly heavily deformed multiyear ice; we have already found (Wadhams, 1988) that undeformed multiyear ice has a unique topography of bulges or blisters which enable this ice type to be distinguished unequivocally from smooth undeformed first-year ice by the use of the sidescan.

Some inferences can be made by contrasting the signatures from the various sensors using the SAR as a convenient reference.

(1) The sonar profile (Figure 2a) beneath the lead has a "grassy" appearance on its left hand side, a result of the strong echo at the water-air interface saturating the recorder. The lead is also well defined in the sidescan sonar image as well as in the PRT-5 and AOL ice topographic profiles. The PRT-5 profile shows the elevated temperature (about -2°C) expected for an open lead while the AOL profile has a fine-scale characteristic of open water. The AMMR brightness temperatures of the lead at 18 GHz (vertical polarization) are low compared to those of consolidated ice. However, the brightness temperatures at 37 GHz do not show similar contrast between open water and ice because of significantly more internal scattering in the ice at 37 GHz than at 18 GHz (Comiso, 1986).

(2) The sensors show that the right side of the lead has been re-frozen. This distinction can be seen in the SAR image which has been enhanced to show contrast between the low image tone values. The contrast between the open water and refrozen lead is very difficult to determine from the SAR image because open water, young ice, and first-year ice all have low backscatter levels. Distinction between the open water and these ice types is considerably more apparent in the sonar, infra-red, and passive microwave records but is somewhat less distinct in the laser record due to the lack of relief between the targets.

(3) A positive correlation is apparent between backscatter level on the SAR image and ice thickness indicated from the sonar and lidar profiles.

(4) Interesting information can also be gathered by comparing the laser topographic profile with the sonar profile and sidescan records even though the

two profiles are offset by some 300 m. Note particularly the shape of the large pressure ridge immediately west of the open lead. The ridge is quite jagged in appearance on the laser record with a height of 3.3 m and width of 100 m, while the corresponding keel is 27 m deep, more rounded, and broader (150 m). The sidescan indicates an area of continuous ridging extending for about 600 m to the west of the lead (confirmed by the high SAR brightness values) while the upward sonar and laser both show that the first ridge in the sequence is the biggest. If we assume that this ridge does not change character between these two profiles, then we can say that the width of the keel is 1.5 times that of the sail and its height 8.2 times the height of the sail. This is within the range of variability of ridges which have been investigated by drilling (e.g. Kovaks and Mellor, 1974) and fits almost exactly a laser-sonar ridge regression found in an earlier experiment (Wadhams, 1981, eqn. 18); the small width multiplier suggests a shear ridge rather than a pressure ridge.

A distinction between the upper and lower ice surfaces can be seen by comparing probability density functions (PDFs) of the laser and sonar profile across the 7 km of track which are shown in Figure 2. The results are shown in Figure 3. It is clear that the distributions are non-gaussian. The greater breadth of the subsurface PDF over the narrower surface PDF is also apparent. The median depth of the sonar PDF is 5.38 m and the mean depth 6.34 m, while the median elevation of the laser PDF is 0.44 m and the mean 0.60 m. The ratios of means are distinctly greater than the sail to keel ratios apparent in the Figure 2 profiles, and may reflect the fact that the tracks were not identical. Figure 3b is a PDF of the SAR brightness values along the same 7 km of track as the laser (Figure 3a), while Figure 3d is the SAR PDF along the same track as

the sonar (Figure 3c).

3.3. Quantitative relationships

SAR pixels have an effective resolution of 5.6m (along track) x 16m (across track). The SAR pixels on original images were subsampled along track by three in order to obtain 16.8m x 16m pixels, which makes it easier for submarine and aircraft tracks to be colocated accurately and for sonar data to be compared with SAR. The original SAR brightness data, each sub-sample and the mean brightness of three sub-samples, were compared. There was no significant difference between the statistics and pdfs of these five series. It was concluded that obtaining 'square pixels' by sub-sampling would not materially affect results.

There is a clear similarity between the shapes of the SAR pdf and the corresponding laser or sonar pdfs, and we have already seen in Figure 2 how there appears to be a strong correspondence between SAR brightness and ice draft or elevation. We investigated this correspondence quantitatively as follows. The laser and sonar data were filtered so as to have the same effective resolution as the sub-sampled SAR pixels (16.8m). Preliminary work had shown that the residuals of linear regressions between SAR and laser and between SAR and sonar data, were not normally distributed and the original data required transforming (normalising) in order to validate regression analyses (Draper and Smith, 1981). In this case square root (sqrt) transformation yielded normal residuals for the SAR brightnesses and sonar drafts, while a fourth root transformation was required to yield normal residuals for the laser.

The resulting relationship (Figures 3e and 3f) is shown as a pair of

scatter diagrams. Figure 3e shows the relationship between sqrt(SAR) brightness and sqrt(ice draft), while Figure 3f relates sqrt(SAR) brightness to fourth root laser elevation [N.B. (ice draft + 1)m is used here because small zero errors in the sonar data can produce negative "drafts" under open leads, which cannot be used for a square root]. The corresponding least squares linear regression lines are also shown. In both cases, the independent variable was SAR brightness (the common data set). The results indicate that, for the single transect studied, the variances explained in transformed laser height and sonar depth by transformed SAR brightness were 15.8% and 17.1% respectively. The regression equation coefficients are not universal, since SAR calibration must be taken into account. Also, the ranges over which these relationships may hold are restricted by the fact that the upper limit of SAR backscatter values is reached at a finite ice draft, so that all greater ice drafts correspond to a saturated SAR brightness.

The results were promising enough to justify a comparison over a longer stretch of track, with the aim of determining an averaging length for SAR brightness and ice draft which will give the best and most useful correlation. Figure 4a shows a 22 km stretch of track, centered on the large lead of Figures 2 and 3, in which the SAR brightness and ice draft are shown together, each smoothed by an 84 m-wide running mean so as to display the main features of the variability more clearly. It can be seen that the peaks and troughs which correspond to identical ridge and lead systems become gradually out of synchronization as distance from the central lead increases. Possible reasons for this are:

(i) The time shift of 3-5 hours between the aircraft and submarine permitted some ice deformation to occur;

(ii) Co-registration is inadequate at these space scales because of continuous fluctuations in aircraft and (especially) submarine speed which are recorded only in a smoothed way by the navigation systems.

We corrected this drift by a linear speed correction to the submarine, having a different slope to left and right of the central lead. The results yielded a correlation coefficient of 0.390 between "square" SAR pixel backscatter and ice draft averaged over the same 16.8 m of track.

With this larger data set we were able to window both SAR and ice draft over n pixels (i.e., an along-track distance of 16.8 n meters), in order to determine the best length scale to use for SAR/draft comparisons. Figure 4b shows the change in correlation coefficient r as n increases. As we might expect, r increases with n, but there is an upper limit to the useful size of n since an excessively long track simply represents average conditions for both surfaces. It was found by inspection of scatter diagrams that the most useful value of n, in which a high correlation coefficient of 0.679 coexists with a substantial point-to-point variability, is 15. This corresponds to an averaging length of 252 m for the top and bottom surfaces. Such a distance is less than that required for the autocorrelation function of the ice bottom to go to zero (Figure 4c), and therefore represents a coherent ice regime for top-to-bottom comparison. The corresponding scatter diagram is shown in Figure 4d. Using this averaging length, the, 46% of the variance in ice draft can be explained in terms of SAR brightness variations.

Actual backscatter / depth relationships are further complicated by other factors, such as the ice roughness, salt content and snow cover. Nonetheless the relationships shown here demonstrate that a basis exists for developing statistics useful for interpreting SAR ice imagery in quantitative terms. The

potential value lies in the possibility that reasonably estimates of ice thickness distribution and variability in the Arctic may be obtained from airborne (or spaceborne) SAR surveys alone.

DISCUSSION

A remote sensing operation in which aircraft and a submarine operate in concert has a unique value, in that it enables validation of passive and active microwave data to be carried out over large areas of ice surface, as opposed to the small number of floes which can be sampled from ice camps. The validation is possible because the submarine sonars give ice draft and ice morphology (from sidescan) information, enabling identification of ice type to be made (Wadhams, 1988). In the sample of data discussed in this paper, we can already see that a potentially useful relationship exists between SAR backscatter and ice draft and elevation. Further correlations will be discussed in future papers.

ACKNOWLEDGMENT

The authors acknowledge the valuable support of the captain, officers and crew of the submarine and aircraft; Cdr I Williams and the staff of Flag Officer Submarines, Northwood; Dr G Burrows and Mr J Carter (Admiralty Research Establishment); Dr E Mollo-Christensen (NASA Goddard) for logistical help and advice; Dr. N Davies (Scott Polar Institute), N Flack and Miss A Scoon (SAIC - Polar Oceans Associates) for data processing; and Dr T Dod for design and installation of microwave radiometers. We are grateful for financial support to the Office of Naval Research under contract N00014-89-C-0014; the National Aeronautics and Space Administration Oceanic Processes Program; the Admiralty Research Establishment, Portland; and the Natural Environment Research Council.

REFERENCES

Comiso, J.C., Characteristics of Arctic winter sea ice from satellite multi-spectral microwave observations. *J. Geophys. Res., 91*, 975-994, 1986.

Draper, N.R. and H. Smith, *Applied Regression Analysis*, New York, Wiley. 1981.

Kovacs, A. and M. Mellor, Sea ice morphology and ice as a geologic agent in the Southern Beaufort Sea, in *The coast and shelf of the Beaufort Sea*, ed. by J.C. Reed and J.E. Sater, Arctic Institute of North America, Arlington, VA, 113-116, 1974.

Tucker III, W.B., A.J. Gow, W.F. Weeks, Physical properties of summer sea ice in the Fram Strait, *J. Geophys. Res., 92*, 6787-6804, 1987.

Wadhams, P., Sea-ice topography of the Arctic Ocean in the region 70°W to 25°E, *Phil. Trans. Roy. Soc., Lond., 302(1464)*, 45-85,1981.

Wadhams, P., The underside of Arctic sea ice imaged by sidescan sonar,. *Nature, 333(6169)*, 161-164, 1988.

FIGURE CAPTIONS

Cover

The front cover provides a composite scene composed of a 50 km by 37 km section of a larger X-band SAR image plotted alongside of a portion of microwave imagery acquired with the NASA ESMR from an altitude of about 6000 m. Obvious correspondence can be seen between the darker first year ice in the SAR image and the signature of the thin ice (colored pink) in the ESMR image. Other notable features that can be discerned between the two remote sensing scenes are areas of thicker and deformed multi-year ice which are seen as lighter areas in the SAR image and darker brown in the ESMR image.

Figure 1. A 40 km section of X-band SAR imagery from north of Greenland. Eastbound (line 1) and westbound (line 2) flight lines of the P-3A aircraft are overlaid on the image, as is the footprint of the AMMR (advanced multichannel microwave radiometer). False color ESMR (electrically scanning microwave radiometer) imagery from lines 1 and 2 is also shown; the flight lines mark the center of the ESMR images which extend so as to just overlap laterally. The box outlined in red shows the location of the imagery and profiles of fig. 2.

Figure 2. A 7 km section of corresponding imagery and profiles. (2a) The SAR brightness levels along the track of the submarine. (2b) The upward sonar profile of ice draft. (2c) Sidescan sonar imagery of the ice underside, with a 1000 m swath width. (2d) Contrast-stretched SAR imagery, with submarine and aircraft tracks overlaid. (2e) The AOL laser profile of ice elevation. (2f) PRT-5 infra-red radiometer profile. (2g) Microwave brightness temperatures from the AMMR.

Figure 3. (a) Probability density function (PDF) of ice elevation from the AOL profile of fig. 2e. (b) PDF of SAR brightness along a track corresponding to the P-3 flight line. (c) PDF of ice draft from the sonar profile of fig. 2b. (d) PDF of SAR brightness along track corresponding to the submarine. (e) Scatter diagram of the square root of SAR brightness versus corresponding square root of ice draft. (f) Scatter diagram of square root of SAR brightness versus fourth root of ice elevation.

Figure 4. (a) SAR brightness level and ice draft plotted together for a 22 km section of track, smoothed over 84 m. (b) Change in correlation between SAR brightness and ice draft as windowing length increases. (c) Autocorrelation function of ice bottom in region covered by fig. 4(a); dotted line is standard error. (d) Scatter diagram of ice draft against SAR brightness, windowed over 15 pixels, with regression line added. Dashed lines are 95% and 99% confidence intervals.

AFFILIATIONS OF AUTHORS

1. Scott Polar Research Institute, University of Cambridge, Cambridge CB2 1ER, England.

2. Laboratory for Oceans, Code 671, NASA Goddard Space Flight Laboratory, Greenbelt, Maryland, 20771.

3. Science Applications International Corporation, Polar Oceans Associates division, Block A2, Westbrook Centre, Milton Road, Cambridge CB4 1YQ, England.

4. Jet Propulsion Laboratory of California Institute of Technology, 4800 Oak Park Drive, Pasadena, California 91109.

5. Admiralty Research Establishment, Southwell, Portland, Dorset, England.

6. NASA Wallops Flight Facility, Wallops Island, Virginia, 23337

7. EG and G Washington Analytical Services Center, P.O. Box 474, Pocomoke City, MD 21851.

8. US Army Cold Regions Research and Engineering Laboratory, 72 Lyme Road, Hanover, New Hampshire 03755.

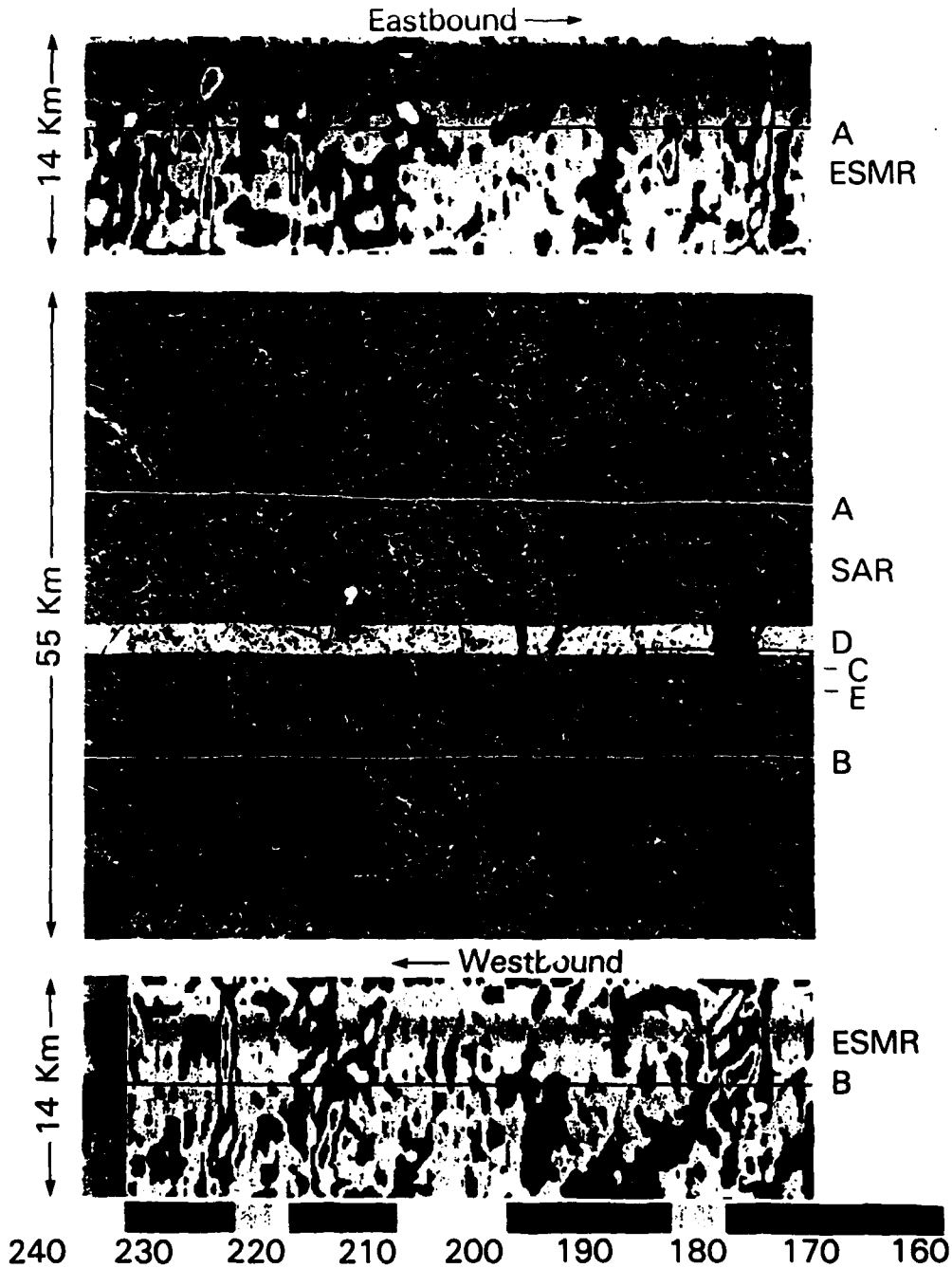

Figure 1. A 40 km section of X-band SAR imagery from north of Greenland. Eastbound (line 1) and westbound (line 2) flight lines of the P-3A aircraft are overlaid on the image, as is the footprint of the AMMR (advanced multichannel microwave radiometer). False color ESMR (electrically scanning microwave radiometer) imagery from lines 1 and 2 is also shown; the flight lines mark the center of the ESMR images which extend so as to just overlap laterally. The box outlined in red shows the location of the imagery and profiles of fig. 2.

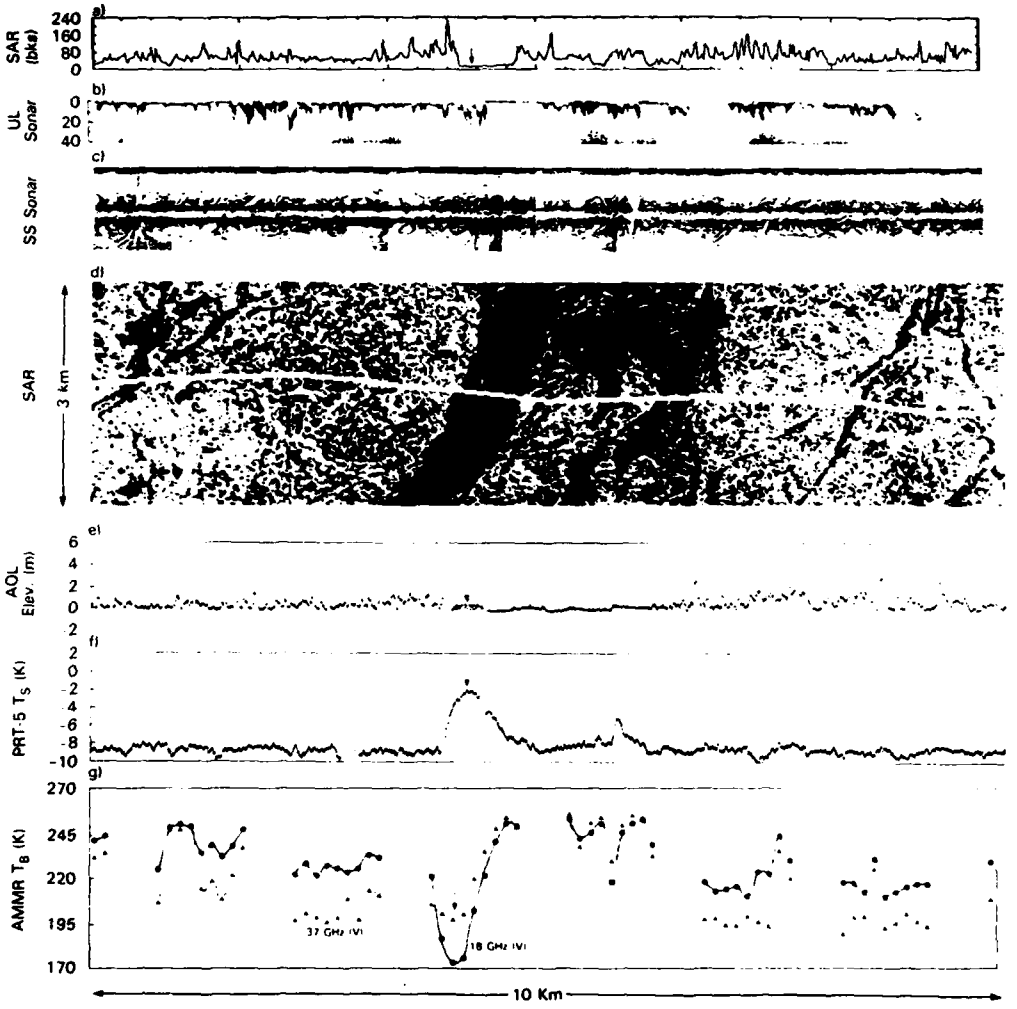

Figure 2. A 7 km section of corresponding imagery and profiles. (2a) The SAR brightness levels along the track of the submarine. (2b) The upward sonar profile of ice draft. (2c) Sidescan sonar imagery of the ice underside, with a 1000 m swath width. (2d) Contrast-stretched SAR imagery, with submarine and aircraft tracks overlaid. (2e) The AOL laser profile of ice elevation. (2f) PRT-5 infra-red radiometer profile. (2g) Microwave brightness temperatures from the AMMR.

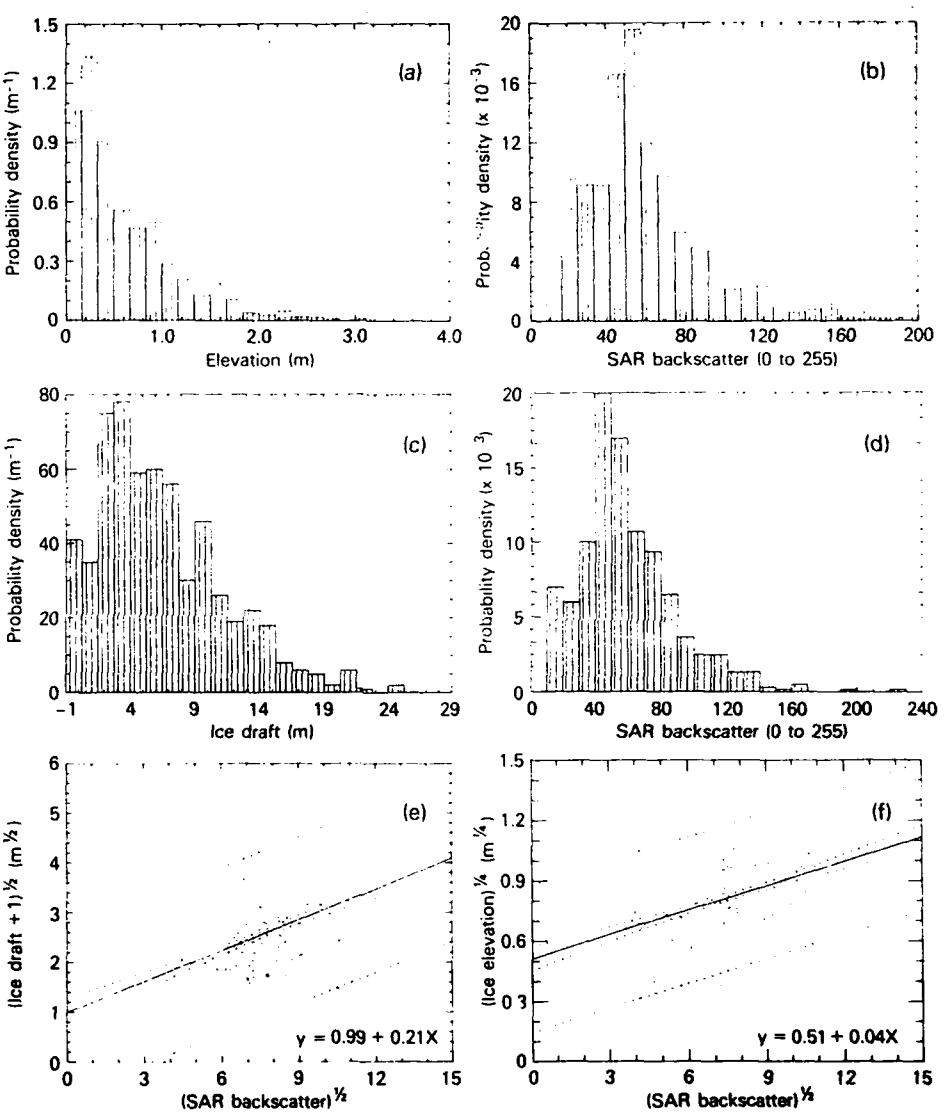

Figure 3. (a) Probability density function (PDF) of ice elevation from the AOL profile of fig. 2e. (b) PDF of SAR brightness along a track corresponding to the P-3 flight line. (c) PDF of ice draft from the sonar profile of fig. 2b. (d) PDF of SAR brightness along track corresponding to the submarine. (e) Scatter diagram of the square root of SAR brightness versus corresponding square root of ice draft. (f) Scatter diagram of square root of SAR brightness versus fourth root of ice elevation.

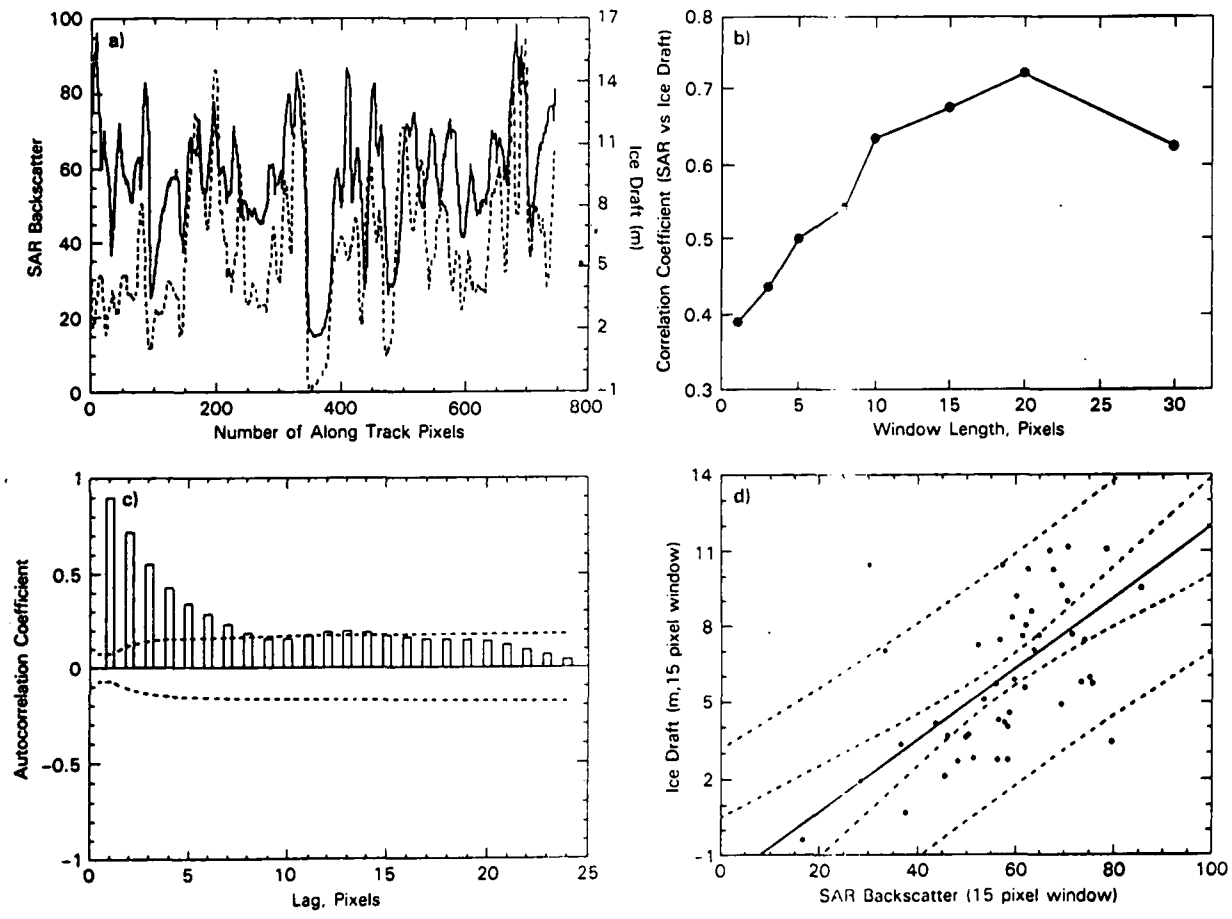

Figure 4. (a) SAR brightness level and ice draft plotted together for a 22 km section of track, smoothed over 84 m. (b) Change in correlation between SAR brightness and ice draft as windowing length increases. (c) Autocorrelation function of ice bottom in region covered by fig. 4(a); dotted line is standard error. (d) Scatter diagram of ice draft against SAR brightness, windowed over 15 pixels, with regression line added. Dashed lines are 95% and 99% confidence intervals